

Primordial non-Gaussianity in the Large Scale Structure of the Universe

Vincent Desjacques^{1,*} and Uroš Seljak^{1,2,†}

¹*Institute for Theoretical Physics, University of Zurich, 8057 Zurich, Switzerland*

²*Physics Department, Astronomy Department and Lawrence Berkeley National Laboratory,
University of California, Berkeley, California 94720, USA*

(Dated: November 8, 2018)

Primordial non-Gaussianity is a potentially powerful discriminant of the physical mechanisms that generated the cosmological fluctuations observed today. Any detection of significant non-Gaussianity would thus have profound implications for our understanding of cosmic structure formation. The large scale mass distribution in the Universe is a sensitive probe of the nature of initial conditions. Recent theoretical progress together with rapid developments in observational techniques will enable us to critically confront predictions of inflationary scenarios and set constraints as competitive as those from the Cosmic Microwave Background. In this paper, we review past and current efforts in the search for primordial non-Gaussianity in the large scale structure of the Universe.

PACS numbers: 98.80.-k, 98.80.Cq

I. INTRODUCTION

In generic inflationary models based on the slow roll of a scalar field, primordial curvature perturbations are produced by the inflaton field as it slowly rolls down its potential [1–4]. Most of these scenarios predict a nearly scale-invariant spectrum of adiabatic curvature fluctuations, a relatively small amount of gravity waves and tiny deviations from Gaussianity in the primeval distribution of curvature perturbations [5–7]. Although the latest measurements of the cosmic microwave background (CMB) anisotropies favor a slightly red power spectrum [8], no significant detection of a B -mode or some level of primordial non-Gaussianity (NG) has thus far been reported from CMB observations.

While the presence of a B -mode can only be tested with CMB measurements, primordial deviations from Gaussianity can leave a detectable signature in the distribution of CMB anisotropies *and* in the large scale structure (LSS) of the Universe. Until recently, it was widely accepted that measurement of the CMB furnish the best probe of primordial non-Gaussianity [9] (see, e.g., the recent review by E. Komatsu on primordial non-Gaussianity in the CMB [10]). However, these conclusions did not take into account the anomalous scale-dependence of the galaxy power spectrum and bispectrum arising from primordial NG of the local $f_{\text{NL}}^{\text{loc}}$ type [11, 12]. These theoretical results, together with rapid developments in observational techniques, will provide large amount of LSS data to critically confront predictions of non-Gaussian models. In particular, galaxy clustering should provide independent constraints on the magnitude of primordial non-Gaussianity as competitive as those from the CMB and, in the long run, may even give the best constraints.

The purpose of this work is to provide an overview of the search for a primordial non-Gaussian signal in the large scale structure. We will begin by briefly summarizing how non-Gaussianity arises in inflationary models (§II). Next, we will discuss the impact of primordial non-Gaussianity on the mass distribution in the low redshift Universe (§III). The main body of this review is §IV, where we describe in detail an number of methods exploiting the abundance and clustering properties of observed tracers of the LSS to constrain the amount of initial non-Gaussianity. We conclude with a discussion of present and forecasted constraints achievable with LSS surveys (§V).

II. MODELS AND OBSERVABLES

Because they assume i) a single dynamical field (the inflaton) ii) canonical kinetic energy terms (i.e. perturbations propagate at the speed of light) iii) slow roll (i.e. the timescale over which the inflaton field changes is much larger than the Hubble rate) iv) an initial vacuum state, single-field slow-roll models lead to a small level of primordial non-Gaussianity [6, 7, 13]. The lowest order statistics sensitive to non-Gaussian features in the initial distribution of scalar perturbations $\Phi(\mathbf{x})$ (we shall adopt the standard CMB convention in which $\Phi(\mathbf{x})$ is the Bardeen’s curvature perturbation in the matter era) is the 3-point function or bispectrum $B_{\Phi}(\mathbf{k}_1, \mathbf{k}_2, \mathbf{k}_3)$, which is a function of any triangle $\mathbf{k}_1 + \mathbf{k}_2 + \mathbf{k}_3 = 0$ (as follows from statistical homogeneity which we assume throughout this paper). It has been recently shown that, in the squeezed limit $k_3 \ll k_1 \approx k_2$, the bispectrum of *any* single-field slow-roll inflationary model asymptotes to the local shape (defined in Eq. 3) [14–16]. The corresponding nonlinear parameter predicted by these models is

$$f_{\text{NL}}^{\text{loc}} = \frac{5}{12} (1 - n_s) \approx 0.017 \quad (\text{single field}) \quad (1)$$

*Electronic address: dvince@physik.uzh.ch

†Electronic address: seljak@physik.uzh.ch

where n_s is the tilt or spectral index of the power spectrum $P_\Phi(k)$, which is accurately measured to be $n_s \approx 0.960 \pm 0.013$ [8]. Therefore, any robust measurement of $f_{\text{NL}}^{\text{loc}}$ well above this level would thus rule out single-field slow-roll inflation.

A. The shape of the primordial bispectrum

Large, potentially detectable amount of Gaussianity can be produced when at least one of the assumptions listed above is violated, i.e. by multiple scalar fields [17, 18], nonlinearities in the relation between the primordial scalar perturbations and the inflaton field [7, 13], interactions of scalar fields [19], a modified dispersion relation or a departure from the adiabatic Bunch-Davies ground state [20]. Generation of a large non-Gaussian signal is also expected at reheating [21] and in the ekpyrotic scenario [22]. Each of these physical mechanisms leaves a distinct signature in the primordial 3-point function $B_\Phi(\mathbf{k}_1, \mathbf{k}_2, \mathbf{k}_3)$, a measurement of which would thus provide a wealth of information about the physics of primordial fluctuations. Although the configuration shape of the primordial bispectrum can be extremely complex in some models, there are broadly three classes of shape characterizing the local, equilateral and folded type of primordial non-Gaussianity [23, 24]. The magnitude of each template ‘‘X’’ is controlled by a dimensionless nonlinear parameter f_{NL}^{X} which we seek to constrain using CMB or LSS observations (instead of attempting a model-independent measurement of B_Φ).

Any non-Gaussianity generated outside the horizon induces a 3-point function that is peaked on squeezed or collapsed triangles for realistic values of the scalar spectral index. The resulting non-Gaussianity depends only on the local value of the Bardeen’s curvature potential, and can thus be conveniently parameterized up to third order by [7, 9, 13, 25]

$$\Phi(\mathbf{x}) = \phi(\mathbf{x}) + f_{\text{NL}}^{\text{loc}} \phi^2(\mathbf{x}) + g_{\text{NL}}^{\text{loc}} \phi^3(\mathbf{x}), \quad (2)$$

where $\phi(\mathbf{x})$ is an isotropic Gaussian random field and $f_{\text{NL}}^{\text{loc}}, g_{\text{NL}}^{\text{loc}}$ are dimensionless, phenomenological parameters. Since curvature perturbations are of magnitude $\mathcal{O}(10^{-5})$, the cubic order correction should always be negligibly small compared to the quadratic one when $\mathcal{O}(f_{\text{NL}}^{\text{loc}}) \sim \mathcal{O}(g_{\text{NL}}^{\text{loc}})$. However, this condition is not satisfied by some multifield inflationary models such as the curvaton scenario, in which a large $g_{\text{NL}}^{\text{loc}}$ and a small $f_{\text{NL}}^{\text{loc}}$ can be simultaneously produced [18]. The quadratic term generates the 3-point function at leading order,

$$B_\Phi^{\text{loc}}(\mathbf{k}_1, \mathbf{k}_2, \mathbf{k}_3) = 2f_{\text{NL}}^{\text{loc}} [P_\phi(k_1)P_\phi(k_2) + (\text{cyc.})], \quad (3)$$

where (cyc.) denotes all cyclic permutations of the indices and $P_\phi(k)$ is the power spectrum of the Gaussian part $\phi(\mathbf{x})$ of the Bardeen potential. The cubic-order terms generates a trispectrum $T_\Phi(\mathbf{k}_1, \mathbf{k}_2, \mathbf{k}_3, \mathbf{k}_4)$ at leading order.

Equilateral type of non-Gaussianity, which arises in inflationary models with higher-derivative operators such as the DBI model, is well described by the factorizable form [26]

$$B_\Phi^{\text{eq}}(\mathbf{k}_1, \mathbf{k}_2, \mathbf{k}_3) = 6f_{\text{NL}}^{\text{eq}} \left[- (P_\phi(k_1)P_\phi(k_2) + (\text{cyc.})) - 2(P_\phi(k_1)P_\phi(k_2)P_\phi(k_3))^{2/3} + (P_\phi^{1/3}(k_1)P_\phi^{2/3}(k_2)P_\phi(k_3) + (\text{perm.})) \right]. \quad (4)$$

It can be easily checked that the signal is largest in the equilateral configurations $k_1 \approx k_2 \approx k_3$, and suppressed in the squeezed limit $k_3 \ll k_1 \approx k_2$. Note that, in single-field slow-roll inflation, the 3-point function is a linear combination of the local and equilateral shape [14].

As a third template, we consider the folded or flattened shape which is maximized for $k_2 \approx k_3 \approx k_1/2$ [27]

$$B_\Phi^{\text{fol}}(\mathbf{k}_1, \mathbf{k}_2, \mathbf{k}_3) = 6f_{\text{NL}}^{\text{fol}} \left[(P_\phi(k_1)P_\phi(k_2) + (\text{cyc.})) + 3(P_\phi(k_1)P_\phi(k_2)P_\phi(k_3))^{2/3} - (P_\phi^{1/3}(k_1)P_\phi^{2/3}(k_2)P_\phi(k_3) + (\text{perm.})) \right]. \quad (5)$$

and approximate the non-Gaussianity due to modification of the initial Bunch-Davies vacuum in canonical single field action (the actual 3-point function is not factorizable). As in the previous example, B_Φ^{fol} is suppressed in the squeezed configurations. Unlike B_Φ^{eq} however, the folded shape induces a scale-dependent bias at large scales (see §IV C).

B. Statistics of the linear mass density field

The Bardeen’s curvature potential $\Phi(\mathbf{x})$ is related to the linear density perturbation $\delta_0(\mathbf{k}, z)$ at redshift z through

$$\delta_0(\mathbf{k}, z) = \mathcal{M}(k, z)\Phi(\mathbf{k}), \quad (6)$$

where

$$\mathcal{M}(k, z) = \frac{2}{3} \frac{k^2 T(k) D(z)}{\Omega_m H_0^2}. \quad (7)$$

Here, $T(k)$ is the matter transfer function normalized to unity as $k \rightarrow 0$, Ω_m is the present-day matter density and $D(z)$ is the linear growth rate normalized to $1 + z$. n -point correlators of the linear mass density field can thus be written as

$$\langle \delta_0(\mathbf{k}) \cdots \delta_0(\mathbf{k}_n) \rangle = \left(\prod_{i=1}^n \mathcal{M}(k_i) \right) \langle \Phi(\mathbf{k}_1) \cdots \Phi(\mathbf{k}_n) \rangle. \quad (8)$$

Smoothing inevitably arises when comparing observations of the large scale structure with theoretical predictions from, e.g., perturbation theory (PT) which are

valid only in the weakly nonlinear regime [28], or from the spherical collapse model which ignores the strongly nonlinear internal dynamics of the collapsing regions [29, 30]. For this reason, we introduce the *smoothed* linear density field

$$\delta_R(\mathbf{k}, z) = \mathcal{M}(k, z)W_R(k)\Phi(\mathbf{k}) \equiv \mathcal{M}_R(k, z)\Phi(\mathbf{k}), \quad (9)$$

where $W_R(k)$ is a (spherically symmetric) window function of characteristic radius R or mass scale M that smoothes out the small-scale nonlinear fluctuations. We will assume a top-hat filter throughout. Furthermore, since M and R are equivalent variables, we shall indistinctly use the notation δ_R and δ_M in what follows.

C. Topological defects models

In addition to inflationary scenarios, there is a whole class of models, known as topological defect models, in which cosmological fluctuations are sourced by an inhomogeneously distributed component which contributes a small fraction of the total energy momentum tensor [31, 32]. The density field is obtained as the convolution of a discrete set of points with a specific density profile. Defects are deeply rooted in particle physics as they are expected to form at a phase transition. Since the early Universe may have plausibly undergone several phase transitions, it is rather unlikely that no defects at all were formed. Furthermore, high redshift tracers of the LSS may be superior to CMB at finding non-Gaussianity sourced by topological defects [33]. However, CMB observations already provide stringent limits on the energy density of a defect component [8], so we shall only minimally discuss the imprint of these scenarios in the large scale structure. Phenomenological defect models are for instance

$$\delta(\mathbf{x}) = \phi(\mathbf{x}) + \alpha_{\text{NL}} (\phi^2(\mathbf{x}) - \langle \phi^2 \rangle) \quad (10)$$

in which the initial matter density $\delta(\mathbf{x})$ (rather than the curvature perturbation $\Phi(\mathbf{x})$) contains a term proportional to the square of a Gaussian scalar field $\phi(\mathbf{x})$ [9], or the χ^2 model (also known as isocurvature CDM model) in which $\delta(\mathbf{x}) \propto \phi^2(\mathbf{x})$ [34].

III. EVOLUTION OF THE MATTER DENSITY FIELD WITH PRIMORDIAL NG

In this Section, we summarize a number of results relative to the effect of primordial NG on the mass density field. These will be useful to understand the complexity that arises when considering biased tracers of the density field (see §IV).

A. Setting up non-Gaussian initial conditions

Investigating the impact of non-Gaussian initial conditions (ICs) on the large scale structure traced by galaxies etc. requires simulations large enough so that many long wavelength modes are sampled. At the same time, the simulations should resolve dark matter halos hosting luminous red galaxies (LRGs) or quasars (QSOs), so that one can construct halo samples whose statistical properties mimic as closely as possible those of the real data. This favors the utilization of pure N-body simulations for which a large dynamical range can be achieved.

The evolution of the matter density field with primordial non-Gaussianity has been studied in series of large cosmological N-body simulations seeded with Gaussian and non-Gaussian initial conditions, see e.g. [12, 35–44]. For generic non-Gaussian (scalar) random fields, we face the problem of setting up numerical simulations with a prescribed correlation structure [45]. While an implementation of the equilateral and folded bispectrum shape requires the calculation of several computationally demanding convolutions, the operation is straightforward for primordial NG described by a local mapping such as the χ^2 or the $f_{\text{NL}}^{\text{loc}}$ model. In the latter case, the local transformation $\Phi = \phi + f_{\text{NL}}^{\text{loc}}\phi^2$ is performed before multiplication by the matter transfer function $T(k)$ (computed with publicly available Boltzmann codes [46, 47]). The (dimensionless) power spectrum of the Gaussian part $\phi(\mathbf{x})$ of the Bardeen potential is the usual power-law $\Delta_\phi^2(k) \equiv k^3 P_\phi(k)/(2\pi^2) = A_\phi(k/k_0)^{n_s-1}$. Unless otherwise stated, we shall assume a normalization $A_\phi = 7.96 \times 10^{-10}$ at the pivot point $k_0 = 0.02 \text{Mpc}^{-1}$. To date, essentially all numerical studies of structure formation with inflationary non-Gaussianity have implemented the local shape solely, so we will focus on this model in what follows.

Non-Gaussian corrections to the primordial curvature perturbations can renormalize the input (unrenormalized) power spectrum of fluctuations used to seed the simulations [48]. For the local $f_{\text{NL}}^{\text{loc}}$ model with $|f_{\text{NL}}^{\text{loc}}| \lesssim 100$, renormalization effects are unlikely to be noticeable due to the limited dynamical range of current cosmological simulations. However, they can be significant, for example, in simulations of a local cubic coupling $g_{\text{NL}}^{\text{loc}}\phi^3$ with a large primordial trispectrum [49]. The cubic order term $g_{\text{NL}}^{\text{loc}}\phi^3$ renormalizes the amplitude A_ϕ of the power spectrum of initial curvature perturbations to $A_\phi \rightarrow A_\phi + 6g_{\text{NL}}^{\text{loc}}\langle \phi^2 \rangle$, where

$$\langle \phi^2 \rangle = \int \frac{d^3k}{(2\pi)^3} P_\phi(k). \quad (11)$$

For scale invariant initial conditions, $\langle \phi^2 \rangle$ has a logarithmic divergence at large and small scales. In practice however, the finite box size and the resolution of the simulations naturally furnish a low- and high- k cutoff. The effective correction to the amplitude of density fluctua-

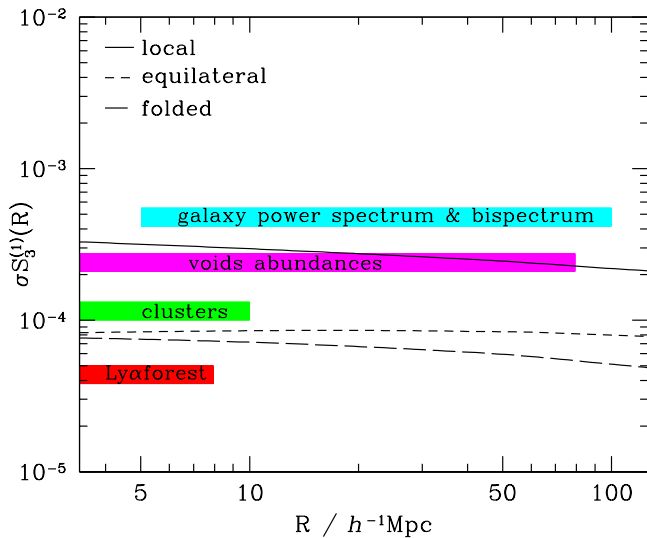


FIG. 1: Skewness $\sigma S_3^{(1)}(R)$ of the smoothed density field in unit of f_{NL}^{X} for the local, equilateral and folded bispectrum shape. The skewness for the equilateral and folded templates is a factor of ~ 3 smaller than in the local model. In any case, this implies that $|\sigma_R S_3(R)| \ll 1$ on the scales probed by the large scale structure for realistic values of the non-linear coupling parameter, $|f_{\text{NL}}^{\text{X}}| \lesssim 100$. The shaded regions approximately indicate the range of scales probed by various LSS tracers. For the galaxy power spectrum and bispectrum, the upper limit sensitively depends upon the surveyed volume.

tions $\delta\sigma_8$ in the $g_{\text{NL}}^{\text{loc}}\phi^3$ model thus is

$$\delta\sigma_8 = 3g_{\text{NL}}^{\text{loc}} \left(\frac{Lk_0}{2\pi}\right)^{1-n_s} [1 - N^{n_s-1}] \frac{A_\phi}{1-n_s}, \quad (12)$$

where N is the number of mesh points along one dimension and L is the simulation box length. For $g_{\text{NL}}^{\text{loc}} = 10^6$, $L = 1.5 h^{-1}\text{Gpc}$ and $N = 1024$ for instance, we obtain $\delta\sigma_8 \approx 0.015$.

To generate the initial particle distribution, the Zelovich approximation is commonly used instead of the exact gravitational dynamics. This effectively corresponds to starting from non-Gaussian initial conditions [50]. Since the transition to the true gravitational dynamics proceeds rather gradually [51], one should ensure that the initial expansion factor is much smaller than that of the outputs analyzed. Alternatively, it is possible to generate more accurate ICs based on second-order Lagrangian perturbation theory (2LPT) [52]. At fixed initial expansion factor, they reduce transients such that the true dynamics is recovered more rapidly [53].

B. Mass density probability distribution

In the absence of primordial NG, the probability distribution function (PDF) of the initial smoothed density

field (the probability that a randomly placed cell of volume V has some specific density) is Gaussian. Namely, all normalized or reduced *smoothed* cumulants S_J of order $J \geq 3$ are zero. An obvious signature of primordial NG would thus be an initially non-vanishing skewness $S_3 = \langle \delta_R^3 \rangle_c / \langle \delta_R^2 \rangle^2$ or kurtosis $S_4 = \langle \delta_R^4 \rangle_c / \langle \delta_R^2 \rangle^3 - 3 / \langle \delta_R^2 \rangle$ [37, 54, 55]. Here, the subscript c denotes the connected piece of the n -point moment that cannot be simplified into a sum over products of lower order moments. At third order for instance, the cumulant of the smoothed density field is an integral of the 3-point function,

$$\langle \delta_R^3 \rangle_c = \int \frac{d^3 k_1}{(2\pi)^3} \int \frac{d^3 k_2}{(2\pi)^3} \int \frac{d^3 k_3}{(2\pi)^3} B_R(\mathbf{k}_1, \mathbf{k}_2, \mathbf{k}_3, z), \quad (13)$$

where

$$B_R(\mathbf{k}_1, \mathbf{k}_2, \mathbf{k}_3, z) = \mathcal{M}_R(k_1, z) \mathcal{M}_R(k_2, z) \mathcal{M}_R(k_3, z) \times B_\Phi(\mathbf{k}_1, \mathbf{k}_2, \mathbf{k}_3) \quad (14)$$

is the bispectrum of the smoothed linear density fluctuations at redshift z . Note that, owing to $S_3(R, z) \propto D(z)^{-1}$, the product $\sigma S_3(R)$ does not depend on redshift. Over the range of scale accessible to LSS observations, $\sigma S_3(R)$ is a monotonic decreasing function of R that is of magnitude $\sim 10^{-4}$ for the local, equilateral and folded templates discussed above (Figure 1). Strictly speaking, all reduced moments should be specified to fully characterize the density PDF, but a reasonable description of the density distribution can be achieved with moments up to the fourth order.

Numerical and analytic studies generally find that a density PDF initially skewed towards positive values produces more overdense regions while a negatively skewed distribution produces larger voids. Gravitational instabilities also generate a positive skewness in the density field, reflecting the fact that the evolved density distribution exhibits an extended tail towards large overdensities [50, 56–60]. This gravitationally-induced signal eventually dominates the primordial contribution such that, at fixed normalization amplitude, non-Gaussian models deviate more strongly from the Gaussian paradigm at high redshift. The time evolution of the normalized cumulants S_J can be worked out for generic Gaussian and non-Gaussian ICs using, e.g., PT or the spherical collapse approximation. For Gaussian ICs, PT predicts the normalized cumulants to be time-independent to lowest non-vanishing order, with a skewness $S_3 \approx 34/7$, whereas for non-Gaussian ICs, the linear contribution to the cumulants decays as $S_J(R, z) = S_J(R, \infty) / D^{J-2}(z)$ [61, 62].

The persistence of the primordial hierarchical amplitude $S_J(R, \infty)$ sensitively depends upon the magnitude of S_N , $N \geq J$, relative to unity. For example, an initially large non-vanishing kurtosis could source skewness with a time-dependence and amplitude similar to that induced by nonlinear gravitational evolution [61]. Although there is an infinite class of non-Gaussian models, we can broadly divide them into weakly and strongly non-Gaussian. In weak NG models, the primeval signal in the

normalized cumulants is rapidly obliterated by gravity-induced non-Gaussianity. This is the case of hierarchical scaling models where n -point correlation functions satisfy $\xi_n \propto \xi_2^{n-1}$ with $\xi_2 \ll 1$ at large scales. By contrast, strongly NG initial conditions dominate the evolution of the normalized cumulants. This occurs when the hierarchy of correlation functions obeys the dimensional scaling $\xi_n \propto \xi_2^{n/2}$, which arises in the particular case of χ^2 initial conditions [63] or in defect models such as texture [38, 64, 65]. These scaling laws have been successfully confronted with numerical investigations of the evolution of cumulants [38, 39]. We note that the scaling of the contribution induced by gravity is, however, different for the kurtosis [66], suggesting that the latter is a better probe of the nature of initial conditions.

Although gravitational clustering tends to erase the memory of initial conditions, numerical simulations of non-Gaussian initial conditions show that the occurrence of highly underdense and overdense regions is very sensitive to the presence of primordial NG. In fact, the imprint of primordial NG is best preserved in the negative tail of the PDF $P(\rho_R)$ of the evolved (and smoothed) density field ρ_R [41]. A satisfactory description of this effect can be obtained from an Edgeworth expansion of the initial smoothed overdensity field [67]. At high densities $\rho_R \gg 1$, the non-Gaussian modification approximately scales as $\rho_R^{3/5}$ whereas, at low densities $\rho_R \simeq 0$, the deviation is steeper, $\rho_R^{6/5}$. Taking into account the weak scale dependence of $\sigma S_3(R)$ further enhances this asymmetry.

C. Power spectrum and bispectrum

Primordial non-Gaussianity also imprints a signature in Fourier space statistics of the matter density field. Positive values of $f_{\text{NL}}^{\text{loc}}$ tend to increase the small scale matter power spectrum $P_\delta(k)$ [11, 41, 68] and the large scale matter bispectrum $B_\delta(\mathbf{k}_1, \mathbf{k}_2, \mathbf{k}_3)$ [11, 69]. In the weakly nonlinear regime where 1-loop PT applies, the Fourier mode of the density field for growing-mode initial conditions reads [57, 70]

$$\delta(\mathbf{k}, z) = \delta_0(\mathbf{k}, z) + \frac{1}{(2\pi)^3} \int d^3q_1 d^3q_2 \delta_{\text{D}}(\mathbf{k} - \mathbf{q}_1 - \mathbf{q}_2) \times F_2(\mathbf{q}_1, \mathbf{q}_2) \delta_0(\mathbf{q}_1, z) \delta_0(\mathbf{q}_2, z). \quad (15)$$

The kernel $F_2(\mathbf{k}_1, \mathbf{k}_2) = 5/7 + \mu(k_1/k_2 + k_2/k_1)/2 + 2\mu^2/7$, where μ is the cosine of the angle between \mathbf{k}_1 and \mathbf{k}_2 , describes the nonlinear 2nd order evolution of the density field. It is nearly independent of Ω_m and Ω_Λ and vanishes in the (squeezed) limit $\mathbf{k}_1 = -\mathbf{k}_2$ as a consequence of the causality of gravitational instability. At 1-loop PT, Eq.(15) generates the mass power spectrum

$$P_\delta(k, z) = P_\delta^{\text{G}}(k, z) + \Delta P_\delta^{\text{NG}}(k, z) = P_0(k, z) + [P_{(22)}(k, z) + P_{(13)}(k, z)] + \Delta P_\delta^{\text{NG}}(k, z). \quad (16)$$

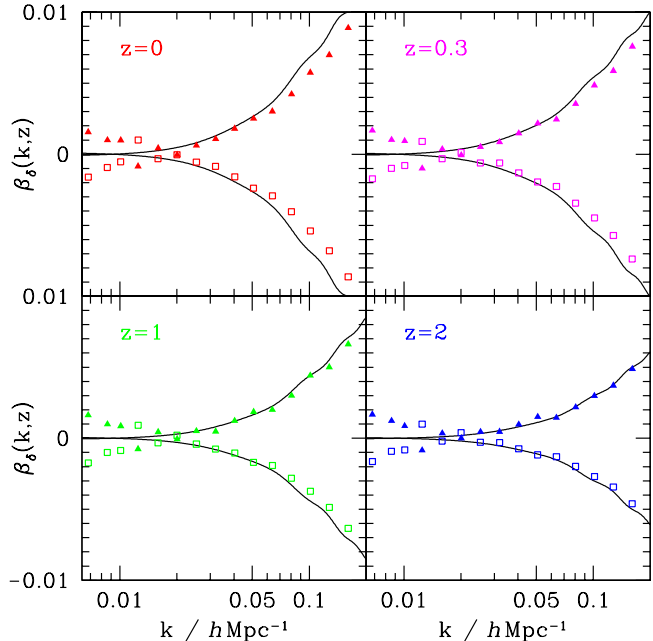


FIG. 2: Non-Gaussian fractional correction $\beta_\delta(k, z) = \Delta P_\delta^{\text{NG}}(k, z)/P_\delta^{\text{G}}(k, z)$ to the matter power spectrum that originates from primordial non-Gaussianity of the local type. Results are shown at redshift $z = 0, 0.5, 1$ and 2 for $f_{\text{NL}}^{\text{loc}} = +100$ (filled symbols) and $f_{\text{NL}}^{\text{loc}} = -100$ (empty symbols). The solid curves indicate the prediction from a 1-loop perturbative expansion.

Here, $P_0(k, z)$ is the linear matter power spectrum at redshift z , $P_{(22)}$ and $P_{(13)}$ are the standard one-loop contributions in the case of Gaussian ICs [70, 71], and

$$\Delta P_\delta^{\text{NG}}(k, z) = 2 \int \frac{d^3q}{(2\pi)^3} F_2(\mathbf{q}, \mathbf{k} - \mathbf{q}) B_0(-\mathbf{k}, \mathbf{q}, \mathbf{k} - \mathbf{q}, z) \quad (17)$$

is the correction due to primordial NG [68]. This term scales as $\propto D^3(z)$, so the effect of non-Gaussianity is largest at low redshift. Moreover, because $F_2(\mathbf{k}_1, \mathbf{k}_2)$ vanishes in the squeezed limit, Eq.(17) is strongly suppressed at small wavenumbers, even in the local $f_{\text{NL}}^{\text{loc}}$ model for which $B_0(-\mathbf{k}, \mathbf{q}, \mathbf{k} - \mathbf{q}, z)$ is maximized in the same limit (i.e. $|\mathbf{k}| \rightarrow 0$). For $f_{\text{NL}}^{\text{loc}} \sim \mathcal{O}(10^2)$, the magnitude of this correction is at a per cent level in the weakly nonlinear regime $k \lesssim 0.1 \text{ hMpc}^{-1}$ [42, 44, 72], in good agreement with the measurements (see Figure 2). Extensions of the renormalization group description of dark matter clustering [73] to non-Gaussian initial density and velocity perturbations can improve the agreement up to wavenumbers $k \lesssim 0.25 \text{ hMpc}^{-1}$ [74, 75].

It is also instructive to compare measurements of the matter bispectrum $B_\delta(k_1, k_2, k_3)$ with perturbative predictions. To second order in PT, the matter bispectrum is the sum of a primordial contribution and two terms induced by gravitational instability [57, 76] (we will hence-

forth omit the explicit z -dependence for brevity),

$$\begin{aligned}
 B_\delta(\mathbf{k}_1, \mathbf{k}_2, \mathbf{k}_3) &= B_0(\mathbf{k}_1, \mathbf{k}_2, \mathbf{k}_3) \\
 &+ \left[2F_2(\mathbf{k}_1, \mathbf{k}_2)P_0(k_1)P_0(k_2) + (\text{cyc.}) \right] \\
 &+ \int \frac{d^3q}{(2\pi)^3} \left[F_2(\mathbf{q}, \mathbf{k}_3 - \mathbf{q}) \right. \\
 &\quad \left. \times T_0(\mathbf{q}, \mathbf{k}_3 - \mathbf{q}, \mathbf{k}_1, \mathbf{k}_2) + (\text{cyc.}) \right],
 \end{aligned} \tag{18}$$

where $T_0(\mathbf{k}_1, \mathbf{k}_2, \mathbf{k}_3, \mathbf{k}_4)$ is the primordial trispectrum of the density field. A similar expression can also be derived for the matter trispectrum, which turns out to be less sensitive to gravitationally induced nonlinearities [77]. The reduced bispectrum Q_3 is conveniently defined as

$$Q_3(\mathbf{k}_1, \mathbf{k}_2, \mathbf{k}_3) = \frac{B_\delta(\mathbf{k}_1, \mathbf{k}_2, \mathbf{k}_3)}{\left[P_\delta(k_1)P_\delta(k_2) + \text{cyclic} \right]}. \tag{19}$$

For Gaussian initial conditions, Q_3 is independent of time and, at tree-level PT, is constant and equal to $Q_3(k, k, k) = 4/7$ for equilateral configurations [57]. For general triangles moreover, it approximately retains this simple behavior, with a dependence on triangle shape through $F_2(\mathbf{k}_1, \mathbf{k}_2)$ [11]. Figure 3 illustrates the effect of primordial NG of the local $f_{\text{NL}}^{\text{loc}}$ type on shape dependence of Q_3 for a particular set of triangle configurations. As can be seen, the inclusion of 1-loop corrections greatly improve the agreement with the numerical data [78]. An important feature that is not apparent in Fig.3 is the fact that the primordial part to the reduced matter bispectrum scales as $Q_3 \propto 1/\mathcal{M}_R(k)$ for approximately equilateral triangles (and under the assumption that $f_{\text{NL}}^{\text{loc}}$ is scale-independent) [11]. This anomalous scaling considerably raises the ability of the matter bispectrum to constrain primordial NG of the local $f_{\text{NL}}^{\text{loc}}$ type. Unfortunately, neither the matter bispectrum nor the power spectrum are directly observable with the large scale structure of the Universe. Temperature anisotropies in the redshifted 21cm background from the pre-reionization epoch could in principle furnish a direct measurement of these quantities [79–81], but foreground contamination may severely hamper any detection. Weak lensing is another direct probe of the dark matter, although we can only observe it in projection along the line of sight [82].

As we will see shortly however, this large-scale anomalous scaling is also present in the bispectrum and power spectrum of observable tracers of the large scale structure such as galaxies. It is this unique signature that will make future all-sky LSS surveys competitive with CMB experiments.

D. Velocities

Primordial non-Gaussianity also leaves a signature in the large-scale coherent bulk motions which, in the linear regime, are directly related to the linear density field

[56]. The various non-Gaussian models considered by [83] tend to have lower velocity dispersion and bulk flow than fiducial Gaussian model, regardless of the sign of the skewness. However, while the probability distribution of velocity components is sensitive to primordial NG of the local type, in defect models it can be very close to Gaussian, even when the density field is strongly non-Gaussian, as a consequence of the central limit theorem [84, 85]. In this regards, correlation of velocity differences could provide a better test of non-Gaussian initial conditions [86].

To measure peculiar velocities, one must subtract the Hubble flow from the observed redshift. This requires an estimate of the distance which is only available for nearby galaxies and clusters (although, e.g., the kinetic Sunyaev-Zel'dovich (kSZ) effect could be used to measure the bulk motions of distant galaxy clusters [87]). So far, measurements of the local galaxy density and velocity fields [88] as well as reconstruction of the initial density PDF from galaxy density and velocity data [89] are consistent with Gaussian initial conditions.

IV. LSS PROBE OF PRIMORDIAL NON-GAUSSIANITY

Discrete and continuous tracers of the large scale structure such as galaxies, the Ly α forest, the 21cm hydrogen line etc., provide a distorted image of the matter density field. In CDM cosmologies, galaxies form inside overdense regions [90] and this introduce a bias between the mass and the galaxy distribution [91]. As a result, distinct samples of galaxies trace the matter distribution differently, the most luminous galaxies preferentially residing in the most massive DM halos. This biasing effect, which concerns most tracers of the large scale structure, remains to be fully understood. Models of galaxy clustering assume for instance that the galaxy biasing relation only depends on the local mass density, but the actual mapping could be more complex [92, 93]. Because of biasing, tracers of the large scale structure will be affected by primordial non-Gaussianity in a different way than the mass density field. In this Section, we describe a number of methods exploiting the abundance and clustering properties of biased tracers to constrain the level of primordial NG. We focus on galaxy clustering as it provides the tightest limits on primordial NG (see §V).

A. Halo finding algorithm

Locating groups of bound particles, or DM halos, in simulations is central to the methods described below. In practice, we aim at extracting halo catalogs with statistical properties similar to those of observed galaxies or quasars. This, however, proves to be quite difficult because the relation between observed galaxies and DM halos is somewhat uncertain. Furthermore, there is freedom at

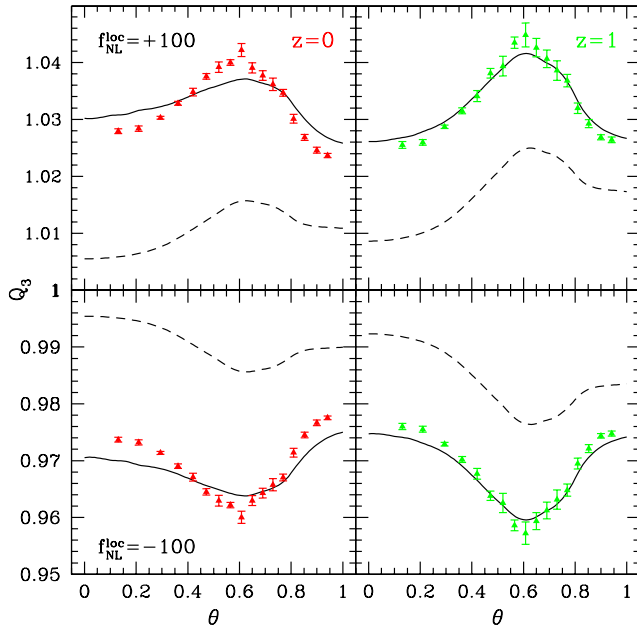


FIG. 3: Reduced matter bispectrum Q_3 as a function of the angle θ between \mathbf{k}_1 and \mathbf{k}_2 for a fixed $k_1 = 0.094 h\text{Mpc}^{-1}$ and $k_2 = 1.5k_1$. The panels show ratios between the non-Gaussian and Gaussian Q_3 for $f_{\text{NL}}^{\text{loc}} = +100$ (top) and -100 (bottom). Dashed lines correspond to tree-level PT while continuous line indicate the 1-loop PT prediction.

defining a halo mass.

A important ingredient is the choice of the halo identification algorithm. Halo finders can be broadly divided into two categories: Friends-of-Friends (FOF) finders [94] and spherical overdensity (SO) finders [95]. While the mass of a SO halo is defined by the radius at which the inner overdensity exceeds $\Delta_{\text{vir}}(z)$ (typically \sim a few hundred times the background density $\bar{\rho}(z)$), the mass of a FOF halo is given by the number of particles within a linking length b from each other ($b \sim 0.15 - 0.2$ in unit of mean interparticle distance) from each other. These definitions are somewhat arbitrary and may suit specific purposes only. In what follows, we shall mainly present results for SO halos as their mass estimate is more closely connected to the predictions of the spherical collapse model, on which most of the analytic formulae presented in this Section are based. The question of how the spherical overdensity masses can be mapped onto friends-of-friends masses remains a matter of debate (e.g. [96]). Clearly however, since the peak height $\nu(M, z)$ depends on the halo mass M through the variance σ_M (see below), any systematic difference will be reflected in the value of ν associated to a specific halo sample. As we will see shortly, this affects the size of the fractional deviation from the Gaussian mass function.

Catalogs of mock galaxies with luminosities comparable to those of the targeted survey provide an additional

layer of complication that can be used, among others, to assess the impact of observational errors on the non-Gaussian signal. However, most numerical studies of cosmic structure formation with primordial NG have not yet addressed this level of sophistication, so we will discuss results based on statistics of dark matter halos only.

B. Abundances of voids and bound objects

It has long been recognized that departure from Gaussianity can significantly affect the abundance of highly biased tracers of the mass density field, as their frequency sensitively depends upon the tails of the initial density PDF [97–99]. The (extended) Press-Schechter approach has been extensively applied to ascertain the effect of primordial NG on the high mass tail of the mass function.

1. Press-Schechter approach

The Press-Schechter theory [100] and its extensions based on excursion sets [101–103] predict that the number density $n(M, z)$ of halos of mass M at redshift z is entirely specified by a multiplicity function $f(\nu)$,

$$n(M, z) = \frac{\bar{\rho}}{M^2} \nu f(\nu) \frac{d \ln \nu}{d \ln M}, \quad (20)$$

where the peak height or significance $\nu(M, z) = \delta_c(z)/\sigma_M$ is the typical amplitude of fluctuations that produce those halos. Here and henceforth, σ_M denotes the variance of the initial density field δ_M smoothed on mass scale $M \propto R^3$ and linearly extrapolated to present epoch, whereas $\delta_c(z) \approx 1.68D(0)/D(z)$ is the critical linear overdensity for (spherical) collapse at redshift z . In the standard Press-Schechter approach, $n(M, z)$ is related to the level excursion probability $P(> \delta_c, M)$ that the linear density contrast of a region of mass M exceeds $\delta_c(z)$,

$$\nu f(\nu) = -2 \frac{\bar{\rho}}{M} \frac{dP}{dM} = \sqrt{\frac{2}{\pi}} \nu e^{-\nu^2/2} \quad (21)$$

where the last equality assumes Gaussian initial conditions. The factor of 2 is introduced to account for the contribution of low density regions embedded in overdensities at scale $> M$. In the extended Press-Schechter theory, δ_M evolves with M and $\nu f(\nu)$ is the probability that a trajectory is absorbed by the constant barrier $\delta = \delta_c$ (as is appropriate in the spherical collapse approximation) on mass scale M . In general, the exact form of $f(\nu)$ depends on the barrier shape [104] and the filter shape [105]. Note also that $\int d\nu f(\nu) = 1$, which ensures that all the mass is contained in halos.

Despite the fact that the Press-Schechter mass function overpredicts (underpredicts) the abundance of low (high) mass objects, it can be used to estimate the fractional deviation from Gaussianity. In this formalism,

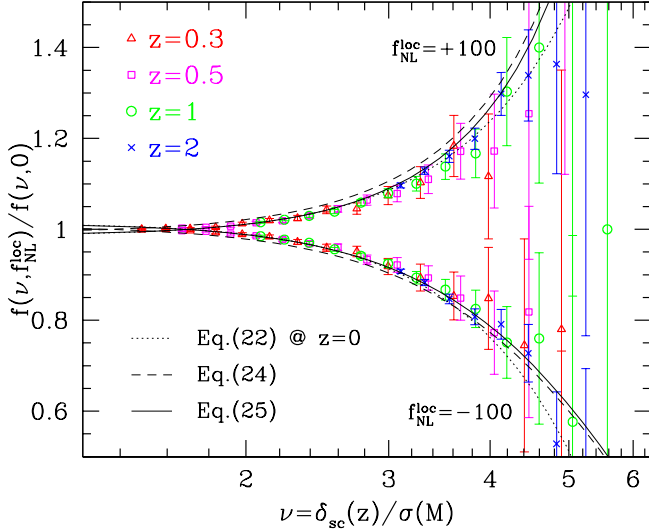


FIG. 4: Fractional deviation from the Gaussian mass function as a function of the peak height $\nu = \delta_c/\sigma$. Different symbols refer to different redshifts as indicated. The various curves are theoretical prediction at $z = 0$ (see text). Halos were identified using a spherical overdensity (SO) finder with a redshift-dependent overdensity threshold $\Delta_{\text{vir}}(z)$ (with $\Delta_{\text{vir}}(z)$ increasing from ~ 200 at high redshift to attain ~ 350 at $z = 0$). Error bars denote Poisson errors. For illustration, $M = 10^{15} M_\odot/h$ corresponds to a significance $\nu = 3.2, 5.2, 7.7$ at redshift $z = 0, 1$ and 2 , respectively. Similarly, $M = 10^{14} M_\odot/h$ and $10^{13} M_\odot/h$ correspond to $\nu = 1.9, 3, 4.5$ and $1.2, 1.9, 2.9$ respectively.

the non-Gaussian fractional correction to the multiplicity function is $R(\nu, f_{\text{NL}}^{\text{X}}) \equiv f(\nu, f_{\text{NL}}^{\text{X}})/f(\nu, 0) = (dP/dM)(> \delta_c, M, f_{\text{NL}}^{\text{X}})/(dP/dM)(> \delta_c, M, 0)$, which is readily computed once the non-Gaussian density PDF $P(\delta_M)$ is known. In the simple extensions proposed by [106] and [107], $P(\delta_M)$ is expressed as the inverse transform of a cumulant generating function. In [107], the saddle-point technique is applied directly to $P(\delta_M)$. The resulting Edgeworth expansion is then used to obtain $P(> \delta_c, M)$. Neglecting cumulants beyond the skewness, one obtain (we momentarily drop the subscript M for convenience)

$$R_{\text{LV}}(\nu, f_{\text{NL}}^{\text{X}}) \approx 1 + \frac{1}{6} \sigma S_3 (\nu^3 - 3\nu) - \frac{1}{6} \frac{d(\sigma S_3)}{d \ln \nu} \left(\nu - \frac{1}{\nu} \right) \quad (22)$$

after integration over regions above $\delta_c(z)$. In [106], it is the level excursion probability $P(> \delta_c, M)$ that is calculated within the saddle-point approximation. This approximation better asymptotes to the exact large mass tail, which exponentially deviates from the Gaussian tail. To enforce the normalization of the resulting mass function, one may define $\nu_\star = \delta_\star/\sigma$ with $\delta_\star = \delta_c \sqrt{1 - S_3 \delta_c/3}$, and use [106, 108]

$$\nu_\star f(\nu_\star) = M^2 \frac{n_{\text{NG}}(M, z)}{\bar{\rho}} \frac{d \ln M}{d \ln \nu_\star}. \quad (23)$$

The fractional deviation from the Gaussian mass function then becomes

$$R_{\text{MVJ}}(\nu, f_{\text{NL}}^{\text{X}}) \approx \exp\left(\frac{\nu^3}{6} \sigma S_3\right) \left[-\frac{\sigma \nu^2}{6 \nu_\star} \frac{d S_3}{d \ln \nu} + \frac{\nu_\star}{\nu} \right]. \quad (24)$$

Both formulae have been shown to give reasonable agreement with numerical simulations of non-Gaussian cosmologies [42, 109, 110] (but note that [12, 111] have reached somewhat different conclusions). Expanding δ_\star at the first order in f_{NL}^{X} shows that these two theoretical expectations differ in the coefficient of the $\nu \sigma S_3$ term. Therefore, it is interesting to consider also the approximation

$$R(\nu, f_{\text{NL}}^{\text{X}}) \approx \exp\left(\frac{\nu^3}{6} \sigma S_3\right) \left[1 - \frac{\nu}{2} \sigma S_3 - \frac{\nu}{6} \frac{d(\sigma S_3)}{d \ln \nu} \right], \quad (25)$$

which is designed to match better the Edgeworth expansion of [107] when the peak height is $\nu \sim 1$ [49]. When the primordial trispectrum is large (i.e. when $g_{\text{NL}}^{\text{loc}} \sim 10^6$), terms involving the kurtosis must be included [49, 106, 107, 112]. In this case, it is also important to take into account a possible renormalization of the fluctuation amplitude, $\sigma_8 \rightarrow \sigma_8 + \delta\sigma_8$ (Eq.12), to which the high mass tail of the mass function is exponentially sensitive [49].

Figure 4 shows the effect of primordial NG of the local $f_{\text{NL}}^{\text{loc}}$ type on the mass function of SO halos identified with a redshift-dependent overdensity threshold $\Delta_{\text{vir}}(z)$ (motivated by spherical collapse in a Λ CDM cosmology [113]). Overall, the approximation Eq.(25) agrees better with the measurements than Eq.(24), which somewhat overestimates the data for $f_{\text{NL}}^{\text{loc}} = 100$, and than Eq.(22), which is not always positive definite for $f_{\text{NL}}^{\text{loc}} = -100$. However, as can be seen in Fig. 5, while the agreement with the data is reasonable for the SO halos, the theory strongly overestimates the effect in the mass function of FOF halos. Reference [110], who use a FOF algorithm with $b = 0.2$, makes the replacement $\delta_c \rightarrow \delta_c \sqrt{q}$ with $q \simeq 0.75$ to match the Gaussian and non-Gaussian mass functions. A physical motivation of this replacement is provided by [114, 115], who demonstrate that the diffusive nature of the collapse barrier introduces a similar factor $q = (1 + D_B)^{-1}$ regardless the initial conditions. However, the value of the diffusion constant D_B was actually measured from simulations that use a SO finder with constant $\Delta_{\text{vir}} = 200$ [116]. In the excursion set approach of [117], the value of q is obtained by normalizing the Gaussian mass function to simulation (i.e. it has nothing to do with the collapse dynamics) and, therefore, depends on the halo finder. Figure 5 demonstrates that this is also the case for the non-Gaussian correction $R(\nu, f_{\text{NL}}^{\text{loc}})$: choosing $q \simeq 0.75$ as advocated in [110] gives good agreement for FOF halos, but strongly underestimates the effect for SO halos, for which the best-fit q is close to unity. As we will see below, the strength of the non-Gaussian bias may also be sensitive to the choice of halo finder.

More sophisticated formulations based on extended Press-Schechter (EPS) theory and/or modifications of the collapse criterion look promising since they can reasonably reproduce both the Gaussian halo counts and the dependence on f_{NL}^{X} [115, 118, 119]. The probability of first upcrossing can, in principle, be derived for any non-Gaussian density field and any choice of smoothing filter [120, 121]. For a general filter, the non-Markovian dynamics generates additional terms in the non-Gaussian correction to the mass function that arise from 3-point correlators of the smoothed density δ_M at different mass scales [115]. However, large error bars still make difficult to test for the presence of such sub-leading terms. For generic moving barriers $B(\sigma)$ such as those appearing in models of triaxial collapse [122, 123], the leading contribution to the non-Gaussian correction approximately is [118]

$$\begin{aligned} R(\nu, f_{\text{NL}}^{\text{X}}) &\approx 1 + \frac{1}{6} \sigma S_3 H_3 \left(\frac{B(\sigma)}{\sigma} \right) \\ &\approx 1 + \frac{1}{6} \sigma S_3 \sqrt{q} (q\nu^3 - 3\nu), \end{aligned} \quad (26)$$

where $H_3(\nu) \equiv \nu^3 - 3\nu$ and the last equality assumes $\nu \gg 1$. For SO halos, Eq.(26) with $q \sim 0.7$ does not fit to the measured correction $R(\nu, f_{\text{NL}}^{\text{loc}})$ better than Eq.(25). However, the ellipsoidal collapse barrier with $q \sim 0.7$ matches better the Gaussian mass function for moderate peak height $\nu \lesssim 2$ [119].

Parameterizations of the fractional correction based on N-body simulations have also been considered. While [43] considers a fourth-order polynomial fit to account for values of $f_{\text{NL}}^{\text{loc}}$ as large as 750, [12] exploits the fact that, for sufficiently small $f_{\text{NL}}^{\text{loc}}$, there is a one-to-one mapping between halos in Gaussian and non-Gaussian cosmologies. In both cases, the fitting functions are consistent with the simulations at the few percent level.

2. Clusters abundance

Rich clusters of galaxies trace the rare, high-density peaks in the initial conditions and thus offer the best probe of the high mass tail of the multiplicity function. To infer the cluster mass function, the X-ray and millimeter windows are better suited than the optical-wave range because selection effects can be understood better (see, however, [124]).

Following early theoretical [97, 98, 125–127] and numerical [36, 128–130] work on the effect of non-Gaussian initial conditions on the multiplicity function of cosmic structures, the abundance of clusters and X-ray counts in non-Gaussian cosmologies has received much attention in the literature. At fixed normalization of the observed abundance of local clusters, the proto-clusters associated with high redshift ($2 < z < 4$) Ly α emitters are much more likely to develop in strongly non-Gaussian models than in the Gaussian paradigm [40, 111, 131]. Considering the redshift evolution of cluster abundances

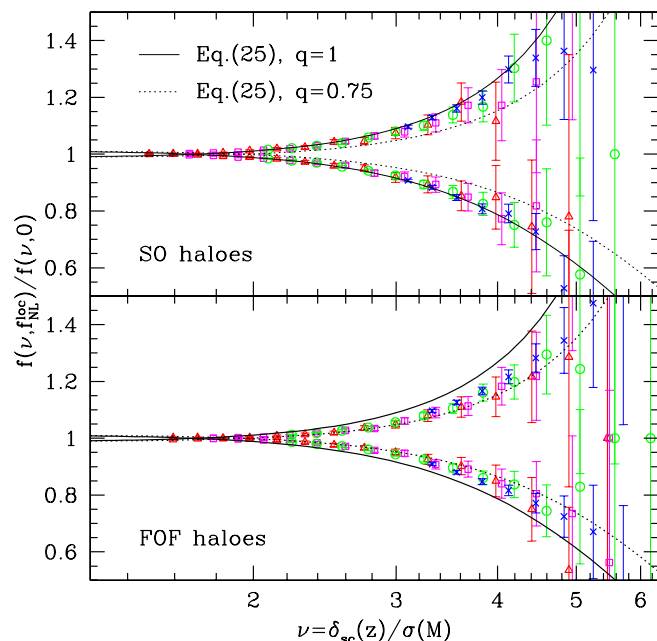


FIG. 5: Fractional deviation from the Gaussian mass function as a function of the peak height $\nu = \delta_c/\sigma$. Different symbols refer to different redshifts as in Fig. 4. The curves are the theoretical prediction Eq. (25) at $z = 0$ with $q = 1$ (solid) and $q = 0.75$ (dotted). In the top panel, halos were identified using a spherical overdensity (SO) finder with a redshift-dependent overdensity threshold $\Delta_{\text{vir}}(z)$ whereas, in the bottom panel, a Friends-of-Friends (FOF) finding algorithm with linking length $b = 0.2$ was used.

thus can break the degeneracy between the initial density PDF and the background cosmology. Simple extensions of the Press-Schechter formalism similar to those considered above have been shown to capture reasonably well the cluster mass function over a wide range of redshift for various non-Gaussian scenarios [132]. Scaling relations between the cluster mass, X-ray temperature and Compton y -parameter calibrated using theory, observations and detailed simulations of cluster formation [133, 134], can be exploited to predict the observed distribution functions of X-ray and SZ signals and assess the capability of cluster surveys to test the nature of the initial conditions [135–141].

An important limitation of this method is that the impact of realistic models of primordial non-Gaussianity on cluster abundances is small compared to systematics in current and upcoming surveys [142–144]. Given the current uncertainties in the redshift evolution of clusters (one commonly assumes that clusters are observed at the epoch they collapse [143]), the selection effects in the calibration of X-ray and SZ fluxes with halo mass, the freedom in the definition of the halo mass, the degeneracy with the normalization amplitude σ_8 (for positive f_{NL}^{X} , the mass function is more enhanced at the high mass end, and this is similar to an increase in the amplitude

of fluctuations σ_8 [145]) and the low number statistics, the prospects of using the cluster mass function only to place competitive limits on f_{NL}^{X} with the current data are small. A two-fold improvement in cluster mass calibration is required to provide constraints comparable to CMB measurements [144].

3. Voids abundance

The frequency of cosmic voids offers a probe of the low density tail of the initial PDF [146]. The Press-Schechter formalism can also be applied to ascertain the sensitivity of the voids abundance to non-Gaussian initial conditions. Voids are defined as regions of mass M whose density is less than some critical value $\delta_v \leq 0$ or, alternatively, whose three eigenvalues of the tidal tensor [147] lie below some critical value $\lambda_v \leq 0$ [67, 119, 146, 148]. An important aspect in the calculation of the mass function of voids is the over-counting of voids located inside collapsing regions. This voids-in-clouds problem, as identified by [149]), can be solved within the excursion set theory by studying a two barriers problem: δ_c for halos and δ_v for voids. Including this effect reduces the frequency of the smallest voids [119]. Neglecting this complication notwithstanding, the differential number density of voids of radius R is [146, 148]

$$\frac{dn}{dR} \approx \frac{9}{2\pi^2} \sqrt{\frac{\pi}{2}} \frac{|\nu_v|}{R^4} e^{-\nu_v^2/2} \frac{d \ln |\nu_v|}{d \ln M} \left[1 - \frac{1}{6} \sigma S_3 H_3(|\nu_v|) \right], \quad (27)$$

where $\nu_v = \delta_v/\sigma_M$. While a positive f_{NL}^{X} produces more massive halos, it generates fewer large voids [119, 146]. Hence, the effect is qualitatively different from a simple rescaling of the normalization amplitude σ_8 . A joint analysis of both abundances of clusters and cosmic voids might thus provide interesting constraints on the shape of the primordial 3-point function. There are, however, several caveats to this method, including the fact that there is no unique way to define voids [146]. Clearly, voids identification algorithms will have to be tested on numerical simulations [150] before a robust method can be applied to real data.

C. Galaxy 2-point correlation

Before [91] showed that, in Gaussian cosmologies, correlations of galaxies and clusters can be amplified relative to the mass distribution, it was argued that primeval fluctuations have a non-Gaussian spectrum [151, 152] to explain the observed strong correlation of Abell clusters [153, 154]. Along these lines, [155] pointed out that primordial non-Gaussianity could significantly increase the amplitude of the two-point correlation of galaxies and clusters on large scales. However, except from [156] who showed that correlations of high density peaks in non-Gaussian models are significantly stronger than in

the Gaussian model with identical mass power spectrum, subsequent work focused mostly on abundances (§IV B) or higher order statistics such as the bispectrum (§IV D). It is only recently that [12] have demonstrated the strong scale-dependent bias arising in non-Gaussian models of the local $f_{\text{NL}}^{\text{loc}}$ type.

1. The non-Gaussian bias

In the original derivation of [12], the Laplacian is applied to the local mapping $\Phi = \phi + f_{\text{NL}}^{\text{loc}} \phi^2$ in order to show that, upon substitution of the Poisson equation, the overdensity in the neighborhood of density peaks is spatially modulated by a factor proportional to the local value of ϕ . Taking into account the coherent motions induced by gravitational instabilities, the scale-dependent bias correction reads

$$\Delta b_\kappa(k, f_{\text{NL}}^{\text{loc}}) = 3f_{\text{NL}}^{\text{loc}} [b_1(M) - 1] \delta_c(0) \frac{\Omega_m H_0^2}{k^2 T(k) D(z)}, \quad (28)$$

where $b_1(M)$ is the linear, Eulerian bias of halos of mass M . This effect can be understood intuitively in terms of a local rescaling of the small-scale amplitude of matter fluctuations or, equivalently, a local rescaling of the critical density threshold [12, 157]. The original result missed out a multiplicative factor of $T(k)^{-1}$ which was introduced subsequently by [158] upon a derivation of Eq. (28) in the limit of high density peaks. The peak-background split approach [104, 159, 160] promoted by [157] shows that the scale-dependent bias applies to any tracer of the matter density field whose (Gaussian) multiplicity function depends on the local mass density only. In this approach, the Gaussian piece of the potential is decomposed into short- and long-wavelength modes, $\phi = \phi_l + \phi_s$. The short-wavelength piece of the density field is then given by the convolution

$$\delta_s = \mathcal{M} \star \Phi_s = \mathcal{M} \star \phi_s (1 + 2f_{\text{NL}}^{\text{loc}} \phi_l) + f_{\text{NL}}^{\text{loc}} \mathcal{M} \star \phi_s^2, \quad (29)$$

where \mathcal{M} is the transfer function Eq.(7). Ignoring the white-noise term, this provides an intuitive explanation of the effect in terms of a local rescaling of the small-scale amplitude of matter fluctuations,

$$\sigma_s \rightarrow \sigma_s \left(1 + 2f_{\text{NL}}^{\text{loc}} \phi_l(\mathbf{x}) \right). \quad (30)$$

Assuming the mass function depends only on the peak height $\nu = \delta_c/\sigma_s$, the long-wavelength part of the halo overdensity becomes [157] (see also [12, 72, 161])

$$\begin{aligned} \delta_l^{\text{h}}(\mathbf{x}) &= \frac{1}{n(\nu)} n \left(\frac{\delta_c - \delta_l(\mathbf{x})}{\sigma_s (1 + 2f_{\text{NL}}^{\text{loc}} \phi_l(\mathbf{x}))} \right) - 1 \quad (31) \\ &\approx -\frac{1}{\sigma_s} \left(\delta_l(\mathbf{x}) + 2f_{\text{NL}}^{\text{loc}} \phi_l(\mathbf{x}) \right) \frac{d \ln n}{d\nu}. \end{aligned}$$

Upon a Fourier transformation and using the fact that, in the Gaussian case, $\delta_l^{\text{h}}(\mathbf{k}) = b_L \delta_l(\mathbf{k})$ with the Lagrangian

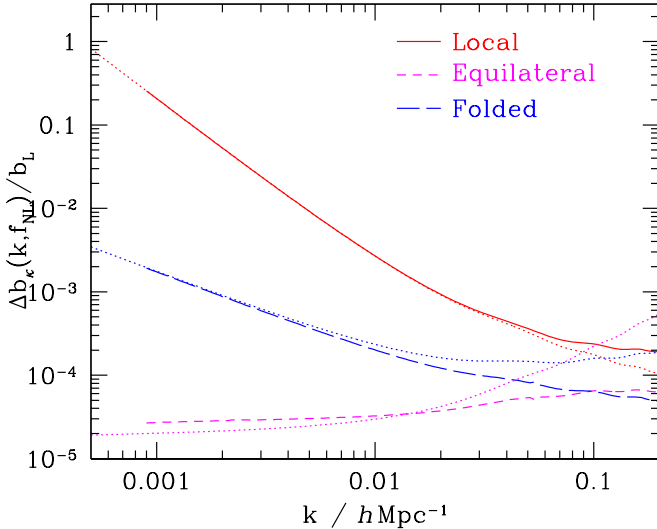


FIG. 6: Non-Gaussian bias correction Eq.(33) for the local, equilateral and folded primordial bispectrum as a function of wavenumber. Results are shown at $z = 0$ for a smoothing radius $R = 5 h^{-1}\text{Mpc}$ and a nonlinear parameter $f_{\text{NL}}^{\text{X}} = 1$. The dotted line represent an analytic approximation, Eqs (35) – (37), which is valid at large scales $k \ll 1$. Note that, while the magnitude of $\Delta b_{\kappa}(k, f_{\text{NL}}^{\text{loc}})$ does not change with R , $\Delta b_{\kappa}(k, f_{\text{NL}}^{\text{eq}})$ and $\Delta b_{\kappa}(k, f_{\text{NL}}^{\text{fol}})$ strongly depends on the smoothing radius (see text).

bias $b_{\text{L}} = -\sigma_s^{-1} d \ln n / d \nu$, we recover the non-Gaussian bias correction Eq.(28) provided that the tracers move coherently with the dark matter, i.e. $b_{\text{L}} = b_1(M) - 1$ [162]. As emphasized in [12], the scale-dependence arises from the fact that the non-Gaussian curvature perturbation $\Phi(\mathbf{x})$ is related to the density through the Poisson equation (6) (so that $\delta_l(\mathbf{k}) = \mathcal{M}(k)\phi_l(\mathbf{k})$). There is no such effect in the (local) χ^2 model, Eq.(10), nor in texture-seeded cosmologies [163] for instance.

The derivation of [158], based on the clustering of regions of the smoothed density field δ_M above threshold $\delta_c(z)$, is formally valid for high density peaks only. However, it is general enough to apply to any shape of primordial bispectrum. The 2-point correlation function of that level excursion set, which was first derived by [125], can be expressed in the high threshold limit ($\nu \gg 1$) as

$$\xi_{>\nu}(\mathbf{r}) = -1 + \exp \left\{ \sum_{n=2}^{\infty} \sum_{j=1}^{n-1} \frac{\nu^n \sigma^{-n}}{j!(n-j)!} \right. \quad (32)$$

$$\left. \times \xi_R^{(n)} \left(\begin{array}{c} \mathbf{x}_1, \dots, \mathbf{x}_1, \\ j \text{ times} \end{array} \quad \begin{array}{c} \mathbf{x}_2, \dots, \mathbf{x}_2 \\ (n-j) \text{ times} \end{array}, z=0 \right) \right\},$$

where $\mathbf{r} = \mathbf{x}_1 - \mathbf{x}_2$. For most non-Gaussian models in which the primordial 3-point function is the dominant correction, this expansion can be truncated at the third order and Fourier transformed to yield the non-Gaussian correction $\Delta P_{>\nu}(k)$ to the power spectrum. Assuming a small level of primordial NG, we can also write

$\Delta P_{>\nu}(k) \approx 2b_{\text{L}}\Delta b_{\kappa}P_R(k)$ where $b_{\text{L}} \approx \nu^2/\delta_c$, and eventually obtain

$$\Delta b_{\kappa}(k, f_{\text{NL}}^{\text{X}}) \equiv b_{\phi}(k)\mathcal{F}(k, f_{\text{NL}}^{\text{X}}) = \left(\frac{2b_{\text{L}}\delta_c(z)}{\mathcal{M}_R(k, 0)} \right) \mathcal{F}(k, f_{\text{NL}}^{\text{X}}). \quad (33)$$

The dependence on the shape of the 3-point function is encoded in the function $\mathcal{F}(k, f_{\text{NL}}^{\text{X}})$ [158, 164],

$$\mathcal{F}(k, f_{\text{NL}}^{\text{X}}) = \frac{1}{16\pi^2\sigma^2} \int_0^{\infty} dk_1 k_1^2 \mathcal{M}_R(k_1, 0) \quad (34)$$

$$\times \int_{-1}^{+1} d\mu \mathcal{M}_R(\sqrt{\alpha}, 0) \frac{B_{\Phi}(k_1, \sqrt{\alpha}, k)}{P_{\Phi}(k)},$$

where $\alpha^2 = k^2 + k_1^2 + 2\mu k k_1$. Note that, for $f_{\text{NL}}^{\text{loc}} < 0$, this first order approximation always breaks down at sufficiently small k because $\Delta P_{>\nu}(k) < 0$.

Figure 6 shows the non-Gaussian halo bias Eq.(33) induced by the local, equilateral and folded bispectrum [164]. In the local and folded non-Gaussianity, the deviation is negligible at $k = 0.1 h\text{Mpc}^{-1}$, but increases rapidly with decreasing wavenumber. Still, the large scale correction is much smaller for the folded template, and nearly absent for the equilateral type, which make them much more difficult to detect with galaxy surveys [164]. To get insights into the behavior of $\Delta b_{\kappa}(k, f_{\text{NL}}^{\text{X}})$ at large scales, let us identify the dominant contribution to $\mathcal{F}(k, f_{\text{NL}}^{\text{X}})$ in the limit $k \ll 1$. Setting $\mathcal{M}_R(\sqrt{\alpha}, 0) \approx \mathcal{M}_R(k_1, 0)$ and expanding $P_{\Phi}(\sqrt{\alpha})$ at second order in k/k_1 , we find after some algebra

$$\mathcal{F}(k, f_{\text{NL}}^{\text{loc}}) \approx f_{\text{NL}}^{\text{loc}} \quad (35)$$

$$\mathcal{F}(k, f_{\text{NL}}^{\text{eq}}) \approx f_{\text{NL}}^{\text{eq}} \left[3 \Sigma_R \left(\frac{2(n_s - 4)}{3} \right) k^{\frac{2(4-n_s)}{3}} \right. \quad (36)$$

$$\left. + \frac{1}{2} (n_s - 4) \Sigma_R(-2) k^2 \right] \sigma_R^{-2}$$

$$\mathcal{F}(k, f_{\text{NL}}^{\text{fol}}) \approx \frac{3}{2} f_{\text{NL}}^{\text{fol}} \Sigma_R \left(\frac{n_s - 4}{3} \right) k^{\frac{4-n_s}{3}} \sigma_R^{-2}, \quad (37)$$

assuming no running scalar index, i.e. $dn_s/d \ln k = 0$. The auxiliary function $\Sigma_R(n)$ is defined as

$$\Sigma_R(n) = \frac{1}{2\pi^2} \int_0^{\infty} dk k^{(2+n)} \mathcal{M}_R(k, 0)^2 P_{\Phi}(k). \quad (38)$$

Hence, we have $\Sigma_R(0) \equiv \sigma_R^2$. As can be seen in Fig. 6, these approximations capture relatively well the large scale non-Gaussian bias correction induced by the equilateral and folded type of non-Gaussianity. For a nearly scale-invariant spectrum $n_s \approx 1$, the effect scales as $\Delta b_{\kappa} \propto k$ and $\Delta b_{\kappa} \propto \text{const.}$, respectively. Another important feature of the equilateral and folded non-Gaussian bias is the dependence on the mass scale M through the multiplicative factor σ_R^{-2} . Indeed, choosing $R = 1 h^{-1}\text{Mpc}$ instead of $R = 5 h^{-1}\text{Mpc}$ as done in Fig. 6 would suppress the effect by a factor of ~ 3 . In the high peak limit, $\sigma_R^{-2} \approx b_{\text{L}}/\delta_c(z)$ which cancels out the dependence on redshift but enhances the sensitivity

to the halo bias, i.e. $\Delta b_\kappa \propto b_L^2$ for the equilateral and folded shapes whereas $\Delta b_\kappa \propto b_L$ in the local model.

At this point, it is appropriate to mention a few caveats to these calculations. Firstly, Eq. (28) assumes that the tracers form after a spherical collapse, which may be a good approximation for the massive halos only. If one instead considers the ellipsoidal collapse dynamics, in which the evolution of a perturbation depends upon the three eigenvalues of the initial tidal shear, $\delta_c(0)$ should be replaced by its ellipsoidal counterparts $\delta_{ec}(0)$ which is always larger than the spherical value [122]. In this model, the scale-dependent bias Δb_κ is thus enhanced by a factor $\delta_{ec}(0)/\delta_c(0)$ [12, 161]. Secondly, Eq. (28) assumes that the biasing of the surveyed objects is described by the peak height ν only or, equivalently, the hosting halo mass M . However, this may not be true for quasars whose activity may be triggered by merger of halos [165, 166]. Reference [157] used the EPS formalism to estimate the bias correction Δb_{merger} induced by mergers,

$$\Delta b_{\text{merger}} = \delta_c^{-1}, \quad (39)$$

so the factor $b_1(M) - 1$ should be replaced by $b_1(M) - 1 - \delta_c^{-1} \approx b_1(M) - 1.6$. The validity of this result should be evaluated with cosmological simulations of quasars formation. In this respect, semi-analytic models of galaxy formation suggest that merger-triggered objects such as quasars do not cluster much differently than other tracers of the same mass [167]. However, this does not mean that the same should hold for the non-Gaussian scale dependent bias. Still, since the recent merger model is an extreme case it seems likely that the actual bias correction is $0 < \Delta b_{\text{merger}} < \delta_c^{-1}$. Thirdly, the scale-dependent bias has been derived using the Newtonian approximation to the Poisson equation, so one may wonder whether general relativistic (GR) corrections to $\mathcal{M}_R(k)^{-1}$ may suppress the effect on scales comparable to the Hubble radius. Reference [168] showed how large scale primordial NG induced by GR corrections propagates onto small scales once cosmological perturbations reenter the Hubble radius in the matter dominated era. This effect generates a scale-dependent bias comparable, albeit of opposite sign to that induced by local NG [164]. More recently, [169] argues that there are no GR corrections to the non-Gaussian bias and that the scaling $\Delta b_\kappa \propto k^{-2}$ applies down to smallish wavenumbers.

We can also ask ourselves whether higher-order terms in the series expansion (32) furnish corrections to the non-Gaussian bias similar to Eq.(28). The quadratic coupling $f_{\text{NL}}^{\text{loc}} \phi^2$ induces a second order correction to the halo power spectrum which reads [49]

$$\begin{aligned} \Delta P_h(k) &= \frac{4}{3} (f_{\text{NL}}^{\text{loc}})^2 [b_1(M) - 1]^2 \delta_c^2(z) S_3^{(1)}(M) \\ &\times \mathcal{M}_R(k, 0) P_\phi(k). \end{aligned} \quad (40)$$

Its magnitude relative to the term linear in $f_{\text{NL}}^{\text{loc}}$, Eq.(28), is approximately 0.03 at redshift $z = 1.8$ and for a halo mass $M = 10^{13} M_\odot/h$. Although its contribution becomes increasingly important at higher redshift, it is

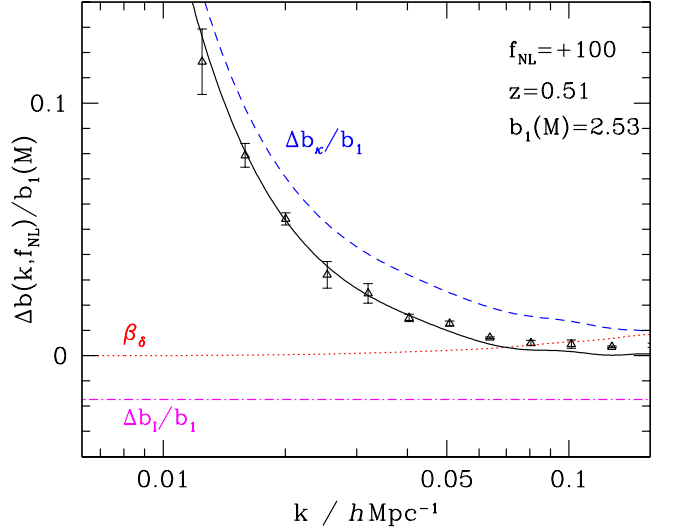


FIG. 7: Non-Gaussian bias correction (filled symbols) for halos of mass $M > 2 \times 10^{13} M_\odot/h$ extracted at $z = 0.5$ from simulations of the local $f_{\text{NL}}^{\text{loc}}$ model. The solid curve represents the theoretical model Eq. (44). The dashed, dotted-dashed-dotted and dotted curves show the scale-dependent bias Δb_κ , the scale-independent offset Δb_1 and the contribution from the matter power spectrum $b_1(M)\beta_\delta$ that arise at first order in $f_{\text{NL}}^{\text{loc}}$ (see Fig.2). The error bars indicate the scatter among 8 realizations of 1024^3 simulations with box size $L = 1600 h^{-1}\text{Mpc}$.

fairly small for realistic values of $f_{\text{NL}}^{\text{loc}}$. In local NG model, the power spectrum of biased tracers of the density field can also be obtained from a local Taylor series in the evolved (Eulerian) density contrast δ and the Gaussian part ϕ of the initial (Lagrangian) curvature perturbation [48, 72]. Using this approach, it can be shown that the halo power spectrum arising from the first order terms of the local bias expansion can be cast into the form [48]

$$P_h(k) = [b_1(M) + f_{\text{NL}}^{\text{loc}} b_\phi(k)]^2 P_R(k) \quad (41)$$

Hence, we also obtain a second order term proportional to $(f_{\text{NL}}^{\text{loc}})^2 \mathcal{M}_R^{-2} P_R(k) = (f_{\text{NL}}^{\text{loc}})^2 P_\phi(k)$ which, however, contributes only at very small wavenumber $k \lesssim 0.001 h^{-1}\text{Mpc}$. All this suggests that Eq. (28) is the dominant contribution to the non-Gaussian bias in the wavenumber range $0.001 \lesssim k \lesssim 0.1 h\text{Mpc}^{-1}$.

Finally, a non-Gaussian, scale-dependent bias correction can also arise in the local, deterministic bias ansatz $\delta_h(\mathbf{x}) = b_1 \delta(\mathbf{x}) + b_2 \delta(\mathbf{x})^2/2 + \dots$ [170] if the initial density field is non-Gaussian. Here, b_N is the N th-order bias parameters (here again, the first-order bias is $b_1 \equiv 1 + b_L$). In this approach, the correction is induced by the correlation $b_1 b_2 \langle \delta(\mathbf{x}_1) \delta^2(\mathbf{x}_2) \rangle$ between the linear and quadratic term in the galaxy biasing relation (which is in fact a collapsed or squeezed 3-point function) and thus reads [68, 69]

$$\Delta b_\kappa(k, f_{\text{NL}}^{\text{loc}}) = 2 f_{\text{NL}}^{\text{loc}} b_2 \sigma_R^2 \mathcal{M}_R(k, 0)^{-1}. \quad (42)$$

Even though $b_2\sigma_R^2 \approx b_L\delta_c$ in the high-threshold limit $\nu \gg 1$, $b_2\sigma_R^2$ behaves very differently than $b_L\delta_c$ for moderate peak height because b_2 is proportional to the second derivative of the mass function $n(\nu)$. So far however, Eq.(28) appears to describe reasonably well the numerical results for a wide range of halo bias.

2. Comparison with simulations

In order to fully exploit the potential of forthcoming large-scale surveys, a number of studies have tested the theoretical prediction against the outcome of large numerical simulations [12, 42–44, 72, 110].

At the lowest order, there are two additional albeit relatively smaller corrections to the Gaussian bias which arise from the dependence of both the halo number density $n(M, z)$ and the matter power spectrum $P_\delta(k, z)$ on primordial NG [42]. Firstly, assuming the peak-background split holds, the change in the mean number density of halos induces a scale-independent offset which we denote $\Delta b_I(f_{\text{NL}}^{\text{loc}})$. In terms of the non-Gaussian fractional correction $R(\nu, f_{\text{NL}}^{\text{loc}})$ to the mass function, this contribution is

$$\Delta b_I(f_{\text{NL}}^{\text{loc}}) = -\frac{1}{\sigma} \frac{\partial}{\partial \nu} \ln \left[R(\nu, f_{\text{NL}}^{\text{loc}}) \right]. \quad (43)$$

It is worth noticing that $\Delta b_I(f_{\text{NL}}^{\text{loc}})$ has a sign opposite to that of $f_{\text{NL}}^{\text{loc}}$, because the bias decreases when the mass function goes up. In practice, the approximation Eq. (25), which matches well the SO data for $\nu \lesssim 4$, can be used for moderate values of the peak height. For FOF halos with linking length $b = 0.2$, one should make the replacement $\delta_c \rightarrow \delta_c\sqrt{q}$ with $q \approx 0.75$ in the calculation of the scale-independent offset. It is sensible to evaluate $\Delta b_I(f_{\text{NL}}^{\text{loc}})$ at a mass scale $\langle M \rangle$ equal to the average halo mass of the sample. Secondly, we also need to account for the change in the matter power spectrum (see Fig. 2 in §III). Summarizing, local non-Gaussianity adds a correction $\Delta b(k, f_{\text{NL}}^{\text{loc}})$ to the bias $b(k)$ of dark matter halos that reads [42]

$$\Delta b(k, f_{\text{NL}}^{\text{loc}}) = \Delta b_\kappa(k, f_{\text{NL}}^{\text{loc}}) + \Delta b_I(f_{\text{NL}}^{\text{loc}}) + b_1(M)\beta_\delta(k, f_{\text{NL}}^{\text{loc}}) \quad (44)$$

at first order in $f_{\text{NL}}^{\text{loc}}$. As can be seen in Fig.7, the inclusion of these extra terms substantially improves the comparison between the theory and the simulations. Considering only the scale-dependent shift Δb_κ leads to an apparent suppression of the effect in simulations relative to the theory. Including the scale-independent offset Δb_I considerably improves the agreement at wavenumbers $k \lesssim 0.05 \text{ hMpc}^{-1}$. Finally, adding the scale-dependent term $b_1(M)\beta_\delta$ further adjusts the match at small scale $k \gtrsim 0.05 \text{ hMpc}^{-1}$ by making the non-Gaussian bias shift less negative. Along these lines, [72] find that the inclusion of Δb_I to the bias also improves the agreement with measurements of $\Delta b(k, f_{\text{NL}}^{\text{loc}})$ obtained for FOF halos, and show that taking into account second- and higher-order

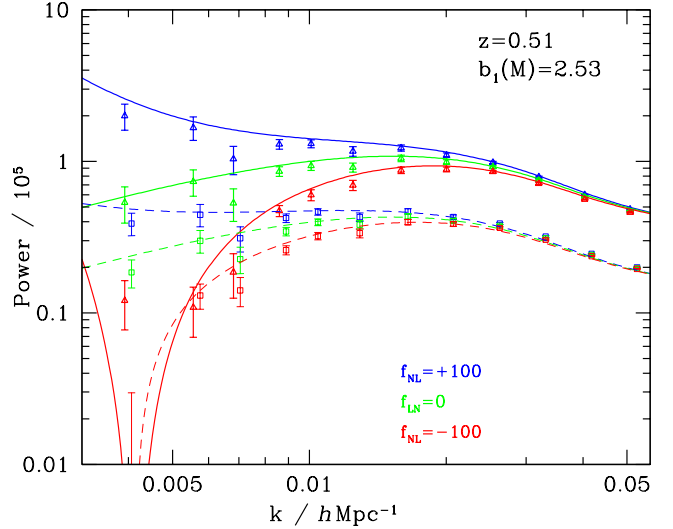


FIG. 8: Halo-halo (solid curve) and halo-matter (dashed curve) power spectra $P_h(k)$ and $P_{h\delta}(k)$ measured in simulations of the Gaussian and $f_{\text{NL}}^{\text{loc}} = \pm 100$ models for halos of mass $M > 2 \times 10^{13} M_\odot/h$ at redshift $z = 1$. The error bars represent the scatter among 8 realizations. For $f_{\text{NL}}^{\text{loc}} = -100$, the cross-power spectrum is negative on scales $k \lesssim 0.005 \text{ hMpc}^{-1}$, in good agreement with the theoretical prediction.

corrections could extend the validity of the theory up to scales $k \sim 0.1 - 0.3 \text{ hMpc}^{-1}$.

The non-Gaussian bias correction can be measured in the cross- and auto-power spectrum of dark matter halos, $P_{h\delta}(k)$ and $P_h(k)$. To compute these quantities, dark matter particles and halo centers are interpolated onto a regular cubical mesh. The resulting dark matter and halo fluctuation fields, $\delta_m(\mathbf{k})$ and $\delta_h(\mathbf{k})$, are then Fourier transformed to yield the matter-matter, halo-matter and halo-halo power spectra $P_\delta(k)$, $P_{h\delta}(k)$ and $P_h(k)$, respectively. $P_h(k)$ is then corrected for the shot noise, which is assumed to be $1/\bar{n}_h$ if dark matter halos are a Poisson sampling of some continuous field. This discreteness correction is negligible for $P_\delta(k)$ due to the large number of dark matter particles. On linear scales ($k \lesssim 0.01 \text{ hMpc}^{-1}$), the halo bias $b(\mathbf{k}) = \delta_h(\mathbf{k})/\delta_m(\mathbf{k})$ approaches the constant value $b_1(M)$ which needs to be measured accurately as it controls the strength of the scale-dependent bias correction Δb_κ . In this respect, the ratio $P_{h\delta}(k)/P_\delta(k)$ is a better proxy for the halo bias since it is less sensitive to shot-noise.

Auto- and cross-power analyses may not agree with each other if the halos and dark matter do not trace each other on scale $k \lesssim 0.01 \text{ hMpc}^{-1}$ where the non-Gaussian bias is large, i.e. if there is stochasticity. Fig.8 shows $P_{h\delta}(k)$ and $P_h(k)$ averaged over 8 realizations of the models with $f_{\text{NL}}^{\text{loc}} = 0, \pm 100$ [42]. The same Gaussian random seed field ϕ was used in each set of runs so as to minimize the sampling variance. Measurements

of the non-Gaussian bias correction obtained with the halo-halo or the halo-matter power spectrum are in a good agreement with each other, indicating that non-Gaussianity does not induce stochasticity and the predicted scaling Eq.(28) applies equally well for the auto- and cross-power spectrum. However, while a number of numerical studies of the $f_{\text{NL}}^{\text{loc}}$ model have confirmed the scaling $\Delta b_{\kappa}(k, f_{\text{NL}}^{\text{loc}}) \propto \mathcal{M}_R(k)^{-1}$ and the redshift dependence $\propto D(z)^{-1}$ [12, 42, 43, 110], the exact amplitude of the non-Gaussian bias correction remains somewhat debatable. Reference [42] who use SO halos and [72] who use FOF halos find satisfactory agreement with the theory once the scale-independent offset Δb_{I} is included. By contrast, [43], who use the same FOF halos as [72], argue that the scale-dependent piece Δb_{κ} requires, among others, a multiplicative correction of the form $(1 - \beta_1 f_{\text{NL}}^{\text{loc}})$, with $\beta_1 \sim 4 \times 10^{-4} > 0$. Similarly, [110] who also use FOF halos find that the theory is a good fit to the simulations only upon replacing b_{L} by qb_{L} in Eq.(33), with $q \simeq 0.75$. Part of the discrepancy may be probably due to the fact that the last two references do not include Δb_{I} , which leads to an apparent suppression of the effect (see Fig.7). Another possible source of discrepancy may be choice of the halo finder which, as seen in Fig.5, has an impact on the strength of the non-Gaussian correction to the mass function. This possibility is investigated in Figure 9, which shows the non-Gaussian bias correction obtained with FOF halos. For this low biased sample, the scale-independent correction is $|\Delta b_{\text{I}}| \lesssim 0.003$ and can thus be neglected. The best-fit values of $f_{\text{NL}}^{\text{loc}}$ are significantly below the input values of ± 100 , in agreement with the findings of [43, 110] (note, however, that this suppression is more consistent with δ_{c} being rescaled by $\sqrt{q}\delta_{\text{c}} \approx 0.86\delta_{\text{c}}$ and b_{L} being unchanged). This indicates that the choice of halo finder may also affect the magnitude of the scale-dependent non-Gaussian bias. Discrepancies have also been observed between the theoretical and measured non-Gaussian bias corrections in non-Gaussian models of the local cubic-order coupling $g_{\text{NL}}^{\text{loc}}\phi^3$ [49]. Understanding all these results clearly requires a better modeling of halo clustering.

3. Redshift-space distortions

Peculiar velocities generate systematic differences between the spatial distribution of data in real and redshift space. These redshift-space distortions must be properly taken into account in order to extract f_{NL}^{X} from redshift surveys. On the linear scales of interest, the redshift-space power spectrum of biased tracers reads as [171, 172]

$$P_{\text{h}}^s(k, \mu) = \left[b_1^2 P_{\delta}(k) + 2b_1 f \mu^2 P_{\delta\theta}(k) + f^2 \mu^4 P_{\theta}(k) \right], \quad (45)$$

where $P_{\delta\theta}$ and P_{θ} are the density-velocity and velocity divergence power spectra, μ is the cosine of the angle between the wavemode \mathbf{k} and the line of sight and f is the logarithmic derivative of the growth factor. For P_{θ} ,

the 1-loop correction due to primordial NG is identical to Eq.(17) provided $F_2(\mathbf{k}_1, \mathbf{k}_2)$ is replaced by the kernel $G_2(\mathbf{k}_1, \mathbf{k}_2) = 3/7 + \mu(k_1/k_2 + k_2/k_1)/2 + 4\mu^2/7$ describing the 2nd order evolution of the velocity divergence [63]. For $P_{\delta\theta}$, this correction is

$$\Delta P_{\delta\theta}^{\text{NG}}(k) = \int \frac{d^3\mathbf{q}}{(2\pi)^3} \left[F_2(\mathbf{q}, \mathbf{k} - \mathbf{q}) + G_2(\mathbf{q}, \mathbf{k} - \mathbf{q}) \right] \times B_0(-\mathbf{k}, \mathbf{q}, \mathbf{k} - \mathbf{q}). \quad (46)$$

Again, causality implies that $G_2(\mathbf{k}_1, \mathbf{k}_2)$ vanishes in the limit $\mathbf{k}_1 = -\mathbf{k}_2$. For unbiased tracers with $b_1 = 1$, the linear Kaiser relation is thus recovered at large scales $k \lesssim 0.01 \text{ hMpc}^{-1}$ (this is consistent with the analysis of [173]). For biased tracers, we still expect the Kaiser formula to be valid, but the distortion parameter β should now be equal to $\beta = f/(b_1 + \Delta b_{\kappa})$, where $\Delta b_{\kappa}(k, f_{\text{NL}}^{\text{X}})$ is the scale-dependent bias induced by the primordial non-Gaussianity.

4. Mitigating cosmic variance and shot-noise

Because of the finite number of large scale wavemodes accessible to a survey, any large scale measurement of the power spectrum is limited by the cosmic (or sampling) variance caused by the random nature of the wave-modes. For discrete tracers such as galaxies, the shot noise is another source of error. Restricting ourselves to weak primordial NG, the relative error on the power spectrum P is $\sigma_P/P \approx 1/\sqrt{N}(1 + \sigma_n^2/P)$, where N is the number of independent modes measured and σ_n^2 is the shot-noise [174]. Under the standard assumption of Poisson sampling, σ_n^2 equals the inverse of the number density $1/\bar{n}$ and causes a scale-independent enhancement of the power spectrum. The extent to which one can improve the observational limits on the nonlinear parameters f_{NL}^{X} will strongly depend on our ability to minimize the impact of these two sources of errors. By comparing differently biased tracers of the same surveyed volume [175, 176] and suitably weighting galaxies (by the mass of their host halo for instance) [177, 178], it should be possible to circumvent these problems and considerably improve the detection level.

Figure 9 illustrates how the impact of sampling variance on the measurement of $f_{\text{NL}}^{\text{loc}}$ can be mitigated. Namely, the data points show the result of taking the ratio $P_{\text{h}}(k, f_{\text{NL}}^{\text{loc}})/P_{\delta}(k, f_{\text{NL}}^{\text{loc}})$ for each set of runs with same Gaussian random seed field ϕ before averaging over the realizations. This procedure is equivalent to the multi-tracers method advocated by [175]. Here, P_{δ} can be thought as mimicking the power spectrum of a nearly unbiased tracer of the mass density field with high number density. Although, in practical applications, using the dark matter field works better [179], in real data P_{δ} should be replaced by a tracer of the same surveyed volume different than the one used to compute P_{h} . Figure 9 also shows that, upon taking out most of the cosmic variance, there is some residual noise caused by the discrete

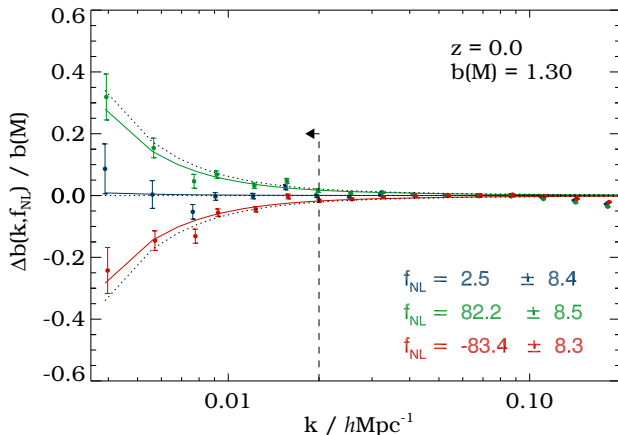


FIG. 9: Fractional correction to the Gaussian halo bias in the $f_{\text{NL}}^{\text{loc}} = \pm 100$ and Gaussian models. In contrast to Fig. 8, halos were identified with a FOF finder of linking length $b = 0.2$. Only the wavenodes to the left of the vertical line were used to fit $\Delta b_{\kappa}(k, f_{\text{NL}}^{\text{loc}})$. For this low biased sample, the scale-independent correction is $|\Delta b_{\text{I}}| \lesssim 0.003$ and can thus be ignored. The best-fit value of $f_{\text{NL}}^{\text{loc}}$ and the corresponding 1σ error is quoted for each model (Figure taken from [179]).

nature of the dark matter halos. As shown recently [178] however, weighting the halos according to their mass can dramatically reduce the shot noise relative to the Poisson expectation, at least when compared against the dark matter. Applying such a weighting may thus significantly improve the error on the nonlinear parameter $f_{\text{NL}}^{\text{loc}}$, but this should be explored in realistic simulations of galaxies, especially because the halo mass M may not be easily measurable from real data [179]. This approach undoubtedly deserves further attention as it has the potential to substantially improve the extraction of the primordial non-Gaussian signal from galaxy surveys.

To conclude this Section, it is worth noting that, while the PDF of power values $P(\mathbf{k})$ has little discriminatory power (for large surveyed volume, it converges towards the Rayleigh distribution as a consequence of the central limit theorem) [180], the covariance of power spectrum measurements (which is sensitive to the selection function, but also to correlations among the phase of the Fourier modes) may provide quantitative limits on certain type of non-Gaussian models [174, 181].

D. Galaxy bispectrum and higher order statistics

Higher statistics of biased tracers, such as the galaxy bispectrum, are of great interest as they are much more sensitive to the shape of the primordial 3-point function than the power spectrum [11, 44, 69, 182, 183]. Therefore, they could break some of the degeneracies affecting the non-Gaussian halo bias (For example, the leading order scale-dependent correction to the Gaussian bias in-

duced by the local quadratic and cubic coupling are fully degenerated [49]).

1. Normalized cumulants of the galaxy distribution

The skewness of the galaxy count probability distribution function could provide constraints on the amount of non-Gaussianity in the initial conditions. As discussed in §III however, it is difficult to disentangle the primordial and gravitational causes of skewness in low redshift data unless the initial density field is strongly non-Gaussian. The first analyzes of galaxy catalogs in terms of count-in-cells densities all reached the conclusion that the skewness (and higher-order moments) of the observed galaxy count PDF is consistent with the value predicted by gravitational instability of initially Gaussian fluctuations [51, 58, 61, 184–186]. Back then however, most of the galaxy samples available were not large enough to accurately determine the S_J at large scales [187]. Despite the two orders of magnitude increase in surveyed volume, these measurements are still sensitive to cosmic variance, i.e. to the presence of massive superclusters or large voids. Nevertheless, the best estimates of the first normalized cumulants S_J of the galaxy PDF strongly suggest that high order galaxy correlation functions indeed follow the hierarchical scaling predicted by the gravitational clustering of Gaussian ICs [188]. There is no evidence for strong non-Gaussianity in the initial density field as might be seeded by cosmic strings or textures [189].

The genus statistics of constant density surfaces through the galaxy distribution measures the relative abundance of low and high density regions as a function of the smoothing scale R and, therefore, could also be used as a diagnostic tool for primordial non-Gaussianity. For a Gaussian random field, the genus curve (i.e. the genus number as a function of the density contrast) is symmetric about $\delta_R = 0$ regardless the value of R . Primordial NG and nonlinear gravitational evolution can disrupt this symmetry [190]. The effect of non-Gaussian ICs on the topology of the galaxy distribution has been explored in a number of papers [36, 191–194]. For large values of R and realistic amount of primordial NG, the genus statistics can also be expanded in a series whose coefficients are the normalized cumulants S_J of the smoothed galaxy density field. In other words, the genus statistics essentially provides another measure of the (large scale) cumulants. So far, measurements from galaxy data are broadly consistent with Gaussian initial conditions [195, 196].

2. Galaxy bispectrum

Most of the scale-dependence of the primordial n -point functions is integrated out in the normalized cumulants, which makes them weakly sensitive to primordial NG.

However, while the effect of non-Gaussian initial conditions, galaxy bias, gravitational instabilities etc. are strongly degenerated in the S_J , they imprint distinct signatures in the galaxy bispectrum $B_g(\mathbf{k}_1, \mathbf{k}_2, \mathbf{k}_3)$, an accurate measurement of which could thus constrain the shape of the primordial 3-point function.

In the original derivation of [182], the large scale (unfiltered) galaxy bispectrum in the $f_{\text{NL}}^{\text{loc}}$ model is given by

$$B_g(\mathbf{k}_1, \mathbf{k}_2, \mathbf{k}_3) = b_1^3 B_0(\mathbf{k}_1, \mathbf{k}_2, \mathbf{k}_3) \quad (47)$$

$$+ b_1^2 b_2 \left[P_0(k_1) P_0(k_2) + (\text{cyc.}) \right]$$

$$+ 2b_1^3 \left[F_2(\mathbf{k}_1, \mathbf{k}_2) P_0(k_1) P_0(k_2) + (\text{cyc.}) \right].$$

Again, b_1 and b_2 are the first- and second-order bias parameters that describe the galaxy biasing relation assumed local and deterministic [170]. The first term in the right-hand side is the primordial contribution which, for equilateral configurations and in the $f_{\text{NL}}^{\text{loc}}$ model, scales as $\mathcal{M}_R(k, z)^{-1}$ like in the matter bispectrum, Eq.(18). The two last terms are the contribution from nonlinear bias and the tree-level correction from gravitational instabilities, respectively. They have the smallest signal in squeezed configurations.

As recognized by [69, 183], Eq.(47) misses an important term that may significantly enhance the sensitivity of the galaxy bispectrum to non-Gaussian initial conditions. This contribution is sourced by the trispectrum $T_R(\mathbf{k}_1, \mathbf{k}_2, \mathbf{k}_3, \mathbf{k}_4)$ of the smoothed mass density field,

$$\frac{1}{2} b_1^2 b_2 \int \frac{d^3 q}{(2\pi)^3} T_R(\mathbf{k}_1, \mathbf{k}_2, \mathbf{q}, \mathbf{k}_3 - \mathbf{q}) + (2 \text{ perms.}) . \quad (48)$$

At large scale, this simplifies to the sum of the linearly evolved primordial trispectrum $T_0(\mathbf{k}_1, \mathbf{k}_2, \mathbf{k}_3, \mathbf{k}_4)$ and a coupling between the primordial bispectrum $B_0(\mathbf{k}_1, \mathbf{k}_2, \mathbf{k}_3)$ (linear in f_{NL}^{X}) and the second order PT corrections (through the kernel $F_2(\mathbf{k}_1, \mathbf{k}_2)$). In the case of local non-Gaussianity and for equilateral configurations, the first piece proportional to T_0 scales as $(f_{\text{NL}}^{\text{loc}})^2 k^{-4}$ times the Gaussian tree-level prediction, with the same redshift dependence. Hence, it is similar to the second order correction $(f_{\text{NL}}^{\text{loc}})^2 \mathcal{M}_R^{-2} P_R(k)$ that appears in the halo power spectrum (see Eq.41). The second piece linear in f_{NL}^{X} generates a signal at large scales for essentially all triangle shapes in the local model as well as in the case of equilateral NG. This second contribution is maximized in the squeezed limit (where it is one order of magnitude larger than the result obtained by [182]) which helps disentangling it from the Gaussian terms. Note that a strong dependence on triangle shape is also present in other NG scenarios such as the χ^2 model [63].

This newly derived contributions are claimed to lead to more than one order of magnitude improvement in certain limits [183], but it is not yet clear whether these gains can be fully realized with upcoming galaxy surveys. To accurately predict the constraints that could be achieved with future measurements of the galaxy bispec-

trum, a comparison of these predictions with the halo bispectrum extracted from numerical simulations is highly desirable. To date, the only numerical study [44] has measured the halo bispectrum for some isosceles triangles ($k_1 = k_2$). While the shape dependence is in reasonable agreement with the theory, the observed k -dependence appears to depart from the predicted scaling.

E. Intergalactic medium and the Ly α forest

Primordial non-Gaussianity also affects the intergalactic medium (IGM) as a positive f_{NL}^{X} enhances the formation of high-mass halos at early times and, therefore, accelerates reionization [197–199]. At lower redshift, small box hydrodynamical simulations of the Ly α forest indicate that non-Gaussian initial conditions could leave a detectable signature in the Ly α flux PDF, power spectrum and bispectrum [200]. However, while differences appear quite pronounced in the high transmissivity tail of the flux PDF (i.e. in underdense regions), the Ly α 1D flux power spectrum seems little affected. Given the small box size of these hydrodynamical simulations, it is worth exploring the effect in large N-body cosmological simulations using a semi-analytic modeling of the Ly α forest [201], even though such an approach only provides a very crude approximation to the temperature-density diagram of the IGM in hydrodynamical simulations. Figure 10 shows the imprint of local type NG on the Ly α 3D flux power spectrum (which is not affected by projection effects) extracted at $z = 2$ from a series of large simulations. The Ly α transmitted flux is calculated in the Gunn-Peterson approximation [202]. A clear signature similar to the non-Gaussian halo bias can be seen. As expected, it is of opposite sign since the Ly α forest is anti-biased relative to the mass density field (overdensities are mapped onto relatively low flux transmission).

To estimate the strength of the signal (see [201] for the details), one can assume that the (real space) optical depth $\tau(\mathbf{x})$ to Ly α absorption at comoving position \mathbf{x} is approximately [203]

$$\tau(\mathbf{x}) = \bar{\tau} \left[1 + \delta_g(\mathbf{x}) \right]^\alpha, \quad (49)$$

where δ_g is the gas density, $\bar{\tau} \sim 1$ is the optical depth at mean gas density and $\alpha \sim 1 - 2$ is some parameter that depends on the exact thermal history of the low density IGM. The above relation holds for the moderate overdensities $\delta_g \lesssim 10$ that are responsible for most of the Ly α absorption features. To relate the gas density to the smoothed linear density field, we could make the simple ansatz $\delta_g \equiv \delta_R$ [204]. In this linear approximation however, the large scale bias b_F of the Ly α flux density field is much larger than that measured in detailed numerical simulations (e.g., $b_F^2 \simeq 0.017$ at $z = 3$ [205]). Therefore, one may want to consider the lognormal mapping [206, 207]

$$1 + \delta_g = \exp(\delta_R - \sigma_R^2/2) \quad (50)$$

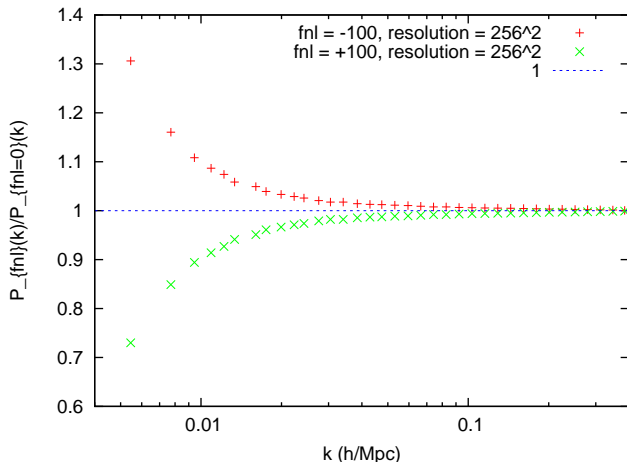


FIG. 10: Ratio between the $z = 2$ Ly α flux power spectrum extracted from simulations of Gaussian and non-Gaussian initial conditions. The mean transmission is set to $\bar{F} = 0.8$ and the power-law exponent $\alpha = 1.65$ (see text).

to better capture nonlinearities in the gas density field. Expanding $\exp(\delta_R)$ at second order and noticing that, in the presence of weak non-Gaussianity, the joint PDF $P(\delta_R(\mathbf{x}_1), \delta_R(\mathbf{x}_2))$ can generically be expanded into an Edgeworth series where the primordial 3-point function is the dominant correction, it is straightforward to compute the Ly α 3D flux power spectrum for nonzero f_{NL}^X . Upon a Fourier transformation, we arrive at

$$\frac{P_{\text{F}}(k, f_{\text{NL}}^X)}{P_{\text{F}}(k, 0)} = 1 - 4g_{\text{F}}\sigma_{\text{R}}^2\mathcal{M}_{\text{R}}(k, z)^{-1}\mathcal{F}(k, f_{\text{NL}}^X). \quad (51)$$

where g_{F} is some auxiliary function of $(\bar{\tau}, \alpha, \sigma_{\text{R}})$. This result is valid for any model of primordial NG characterized by an initial bispectrum. In the $f_{\text{NL}}^{\text{loc}}$ model, the large-scale non-Gaussian Ly α bias scales as $\Delta b_{\text{F}}(k, f_{\text{NL}}^X) \approx -2g_{\text{F}}\sigma_{\text{R}}^2\mathcal{M}_{\text{R}}(k, z)^{-1} \propto k^{-2}T(k)^{-1}$ like the non-Gaussian halo bias. Assuming $\bar{\tau} = 0.7$, $\sigma_{\text{R}} = 1.8$ and $\alpha = 1.65$ yields a mean flux $\bar{F} \approx 0.8$ and a ratio $P_{\text{F}}(k = 0.01, f_{\text{NL}}^X)/P_{\text{F}}(k = 0.01, 0) \approx 1 \mp 0.13$ for $f_{\text{NL}}^{\text{loc}} = \pm 100$ comparable in magnitude to that seen in Fig. 10. A detection of this effect, although challenging in particular because of continuum uncertainties, could be feasible with future data sets. Summarizing, the Ly α should provide interesting information on the non-Gaussian signal over a range of scale and redshift not easily accessible to galaxy and CMB observations [200, 201].

V. CURRENT LIMITS AND PROSPECTS

As the importance of primordial non-Gaussianity relative to the non-Gaussianity induced by gravitational clustering and galaxy bias increases towards high redshift, the optimal strategy to constrain the nonlinear coupling

parameter(s) with LSS is to use large scale, high-redshift observations [33].

A. Existing constraints on primordial NG

The non-Gaussian halo bias presently is the only LSS method that provides a robust limit on the magnitude of a primordial 3-point function of the local shape. It is a broadband effect that can be easily measured with photometric redshifts. The authors of [157] have applied Eq.(28) to constrain the value of $f_{\text{NL}}^{\text{loc}}$ using a compilation of large-scale clustering data. Their constraint arise mostly from the QSO sample at median redshift $z = 1.8$, which covers a large comoving volume and is highly biased, $b_1 = 2.7$. They obtain

$$-29 < f_{\text{NL}}^{\text{loc}} < +69 \quad (52)$$

at 95% confidence level. These limits are competitive with those from CMB measurements, $-10 < f_{\text{NL}}^{\text{loc}} < +74$ [208]. It is straightforward to translate this 2- σ limit into a constraint on the cubic order coupling $g_{\text{NL}}^{\text{loc}}$ since the non-Gaussian scale-dependent bias $\Delta b_{\kappa}(k, g_{\text{NL}}^{\text{loc}})$ has the same functional form as $\Delta b_{\kappa}(k, f_{\text{NL}}^{\text{loc}})$ [49]. Assuming $f_{\text{NL}}^{\text{loc}} = 0$, one obtains

$$-3.5 \times 10^5 < g_{\text{NL}}^{\text{loc}} < +8.2 \times 10^5. \quad (53)$$

These limits are comparable with those inferred from the analysis of CMB data.

Measurements of the galaxy bispectrum in several redshift catalogs have shown evidence for a configuration shape dependence in agreement with that predicted from gravitational instability, ruling out χ^2 initial conditions at the 95% C.L. [209, 210]. Recent analyses of the SDSS LRGs catalogue indicate that the shape dependence of the reduced 3-point correlation $Q_3 \sim \xi_3/(\xi_2)^2$ is also consistent with Gaussian ICs [211], although a primordial (hierarchical) non-Gaussian contribution in the range $Q_3 \sim 0.5 - 3$ cannot be ruled out [212]. Other LSS probes of primordial non-Gaussianity, such as the abundance of massive clusters, are still too affected by systematics to furnish tight constraints on the shape and magnitude of a primordial 3-point function. Still, the observation of a handful of unexpectedly massive high-redshift clusters has been interpreted as evidence of a substantial degree of primordial NG [213–215].

B. Future prospects

Improving the current limits will further constrain the physical mechanisms for the generation of cosmological perturbations.

The non-Gaussian halo bias also leaves a signature in cross-correlation statistics of weak cosmic shear (galaxy-galaxy and galaxy-CMB) [216, 217] and in the integrated Sachs-Wolfe (ISW) effect [157, 161, 218]. Measurements

of the lensing bispectrum could also constrain a number of non-Gaussian models [219]. However, galaxy clustering will undoubtedly offer the most promising LSS diagnostic of primordial non-Gaussianity. The detectability of a local primordial bispectrum has been assessed in a series of papers. It is expected that future all-sky galaxy surveys will achieve constraints of the order of $\Delta f_{\text{NL}}^{\text{loc}} \sim 1$ assuming all systematics are reasonably under control [48, 107, 157, 161, 218, 220–222]. Realistic models of cubic type non-Gaussianity [49], modifications of the initial vacuum state or horizon-scale GR corrections [164] should also be tested with future measurement of the galaxy power spectrum.

Upcoming observations of high redshift clusters will provide increased leverage on measurement of primordial non-Gaussianity with abundances and possibly put limits on any nonlinear parameter f_{NL}^{X} at the level of a few tens [140]. Combining the information provided by the evolution of the mass function and power spectrum of galaxy clusters should yield constraints with a precision $\Delta f_{\text{NL}}^{\text{loc}} \sim 10$ for a wide field survey covering half of the sky [215]. Alternatively, using the full covariance of cluster counts (which is sensitive to the non-Gaussian halo bias) can furnish constraints of $\Delta f_{\text{NL}}^{\text{loc}} \sim 1–5$ for a Dark Energy Survey-type experiment [223, 224].

As emphasized in §IV however, the exact magnitude of the non-Gaussian bias is still uncertain partly due to the freedom at the definition of the halo mass and the uncertainty in the correspondence between simulated quantities and observables. Understanding this type of

systematics will be crucial to set reliable constraints on a primordial non-Gaussian component. To fully exploit the potential of future galaxy surveys, it will also be essential to extend the theoretical and numerical analyses to other bispectrum shapes than the local template used so far. Ultimately, the gain that can be achieved will critically depend on our ability to minimize the impact of sampling variance and shot-noise. In this regards, multi-tracers methods combined with optimal weighting schemes should deserve further attention as they hold the promise to become the most accurate method to extract the primordial non-Gaussian signal from galaxy surveys [175–178].

VI. ACKNOWLEDGMENTS

We give our special thanks to Nico Hamaus and Shirley Ho for sharing with us material prior to publication, and Emiliano Sefusatti for providing us with the data shown in Fig.3. We would also like to thank Martin Crocce, Christopher Hirata, Ilian Iliev, Tsz Yan Lam, Patrick McDonald, Nikhil Padmanabhan, and Anze Slosar for collaboration on these issues, and Tobias Baldauf for comments and for a careful reading of this manuscript. This work was supported by the Swiss National Foundation (Contract No. 200021-116696/1) and made extensive use of the NASA Astrophysics Data System and and arXiv.org preprint server.

-
- [1] V. F. Mukhanov and G. V. Chibisov. Quantum fluctuations and a nonsingular universe. *Soviet Journal of Experimental and Theoretical Physics Letters*, 33:532–+, May 1981.
 - [2] A. A. Starobinsky. Dynamics of phase transition in the new inflationary universe scenario and generation of perturbations. *Physics Letters B*, 117:175–178, November 1982.
 - [3] S. W. Hawking. The development of irregularities in a single bubble inflationary universe. *Physics Letters B*, 115:295–297, September 1982.
 - [4] A. H. Guth and S.-Y. Pi. Fluctuations in the new inflationary universe. *Physical Review Letters*, 49:1110–1113, October 1982.
 - [5] T. J. Allen, B. Grinstein, and M. B. Wise. Non-gaussian density perturbations in inflationary cosmologies. *Physics Letters B*, 197:66–70, October 1987.
 - [6] T. Falk, R. Rangarajan, and M. Srednicki. Dependence of density perturbations on the coupling constant in a simple model of inflation. *Phys. Rev. D.*, 46:4232–4234, November 1992.
 - [7] A. Gangui, F. Lucchin, S. Matarrese, and S. Mollerach. The three-point correlation function of the cosmic microwave background in inflationary models. *Astrophys. J.*, 430:447–457, August 1994.
 - [8] E. Komatsu, J. Dunkley, M. R. Nolta, C. L. Bennett, B. Gold, G. Hinshaw, N. Jarosik, D. Larson, M. Limon, L. Page, D. N. Spergel, M. Halpern, R. S. Hill, A. Kogut, S. S. Meyer, G. S. Tucker, J. L. Weiland, E. Wollack, and E. L. Wright. Five-Year Wilkinson Microwave Anisotropy Probe Observations: Cosmological Interpretation. *ApJS*, 180:330–376, February 2009.
 - [9] L. Verde, L. Wang, A. F. Heavens, and M. Kamionkowski. Large-scale structure, the cosmic microwave background and primordial non-Gaussianity. *Mon. Not. R. Astron. Soc.*, 313:141–147, March 2000.
 - [10] E. Komatsu. Hunting for primordial non-Gaussianity in the cosmic microwave background. *Classical and Quantum Gravity*, 27(12):124010–+, June 2010.
 - [11] R. Scoccimarro, E. Sefusatti, and M. Zaldarriaga. Probing primordial non-Gaussianity with large-scale structure. *Phys. Rev. D.*, 69(10):103513–+, May 2004.
 - [12] N. Dalal, O. Doré, D. Huterer, and A. Shirokov. Imprints of primordial non-Gaussianities on large-scale structure: Scale-dependent bias and abundance of virialized objects. *Phys. Rev. D.*, 77(12):123514–+, June 2008.
 - [13] D. S. Salopek and J. R. Bond. Nonlinear evolution of long-wavelength metric fluctuations in inflationary models. *Phys. Rev. D.*, 42:3936–3962, December 1990.
 - [14] J. Maldacena. Non-gaussian features of primordial fluctuations in single field inflationary models. *Journal of High Energy Physics*, 5:13–+, May 2003.

- [15] V. Acquaviva, N. Bartolo, S. Matarrese, and A. Riotto. Gauge-invariant second-order perturbations and non-Gaussianity from inflation. *Nuclear Physics B*, 667:119–148, September 2003.
- [16] P. Creminelli and M. Zaldarriaga. A single-field consistency relation for the three-point function. *Journal of Cosmology and Astro-Particle Physics*, 10:6–+, October 2004.
- [17] A. Linde and V. Mukhanov. Non-Gaussian isocurvature perturbations from inflation. *Phys. Rev. D.*, 56:535–+, July 1997.
- [18] D. H. Lyth, C. Ungarelli, and D. Wands. Primordial density perturbation in the curvaton scenario. *Phys. Rev. D.*, 67(2):023503–+, January 2003.
- [19] T. Falk, R. Rangarajan, and M. Srednicki. The angular dependence of the three-point correlation function of the cosmic microwave background radiation as predicted by inflationary cosmologies. *Astrophys. J. Lett.*, 403:L1–L3, January 1993.
- [20] J. Lesgourgues, D. Polarski, and A. A. Starobinsky. Quantum-to-classical transition of cosmological perturbations for non-vacuum initial states. *Nuclear Physics B*, 497:479–508, February 1997.
- [21] G. Dvali, A. Gruzinov, and M. Zaldarriaga. Cosmological perturbations from inhomogeneous reheating, freeze-out, and mass domination. *Phys. Rev. D.*, 69(8):083505–+, April 2004.
- [22] J.-L. Lehners and P. J. Steinhardt. Non-Gaussian density fluctuations from entropically generated curvature perturbations in ekpyrotic models. *Phys. Rev. D.*, 77(6):063533–+, March 2008.
- [23] D. Babich, P. Creminelli, and M. Zaldarriaga. The shape of non-Gaussianities. *Journal of Cosmology and Astro-Particle Physics*, 8:9–+, August 2004.
- [24] J. R. Fergusson and E. P. S. Shellard. Shape of primordial non-Gaussianity and the CMB bispectrum. *Phys. Rev. D.*, 80(4):043510–+, August 2009.
- [25] E. Komatsu and D. N. Spergel. Acoustic signatures in the primary microwave background bispectrum. *Phys. Rev. D.*, 63(6):063002–+, March 2001.
- [26] P. Creminelli, A. Nicolis, L. Senatore, M. Tegmark, and M. Zaldarriaga. Limits on non-Gaussianities from WMAP data. *Journal of Cosmology and Astro-Particle Physics*, 5:4–+, May 2006.
- [27] P. D. Meerburg, J. P. van der Schaar, and P. Stefano Corasaniti. Signatures of initial state modifications on bispectrum statistics. *Journal of Cosmology and Astro-Particle Physics*, 5:18–+, May 2009.
- [28] F. Bernardeau, S. Colombi, E. Gaztañaga, and R. Scocimarro. Large-scale structure of the Universe and cosmological perturbation theory. *Phys. Rep.*, 367:1–248, September 2002.
- [29] J. E. Gunn and J. R. Gott, III. On the Infall of Matter Into Clusters of Galaxies and Some Effects on Their Evolution. *Astrophys. J.*, 176:1–+, August 1972.
- [30] J. R. Bond and S. T. Myers. The Peak-Patch Picture of Cosmic Catalogs. I. Algorithms. *ApJS*, 103:1–+, March 1996.
- [31] R. Durrer. Topological defects in cosmology. *New Astronomy Review*, 43:111–156, July 1999.
- [32] A. Vilenkin and E. P. S. Shellard. *Cosmic Strings and Other Topological Defects*. July 2000.
- [33] L. Verde, R. Jimenez, M. Kamionkowski, and S. Matarrese. Tests for primordial non-Gaussianity. *Mon. Not. R. Astron. Soc.*, 325:412–418, July 2001.
- [34] P. J. E. Peebles. An Isocurvature Cold Dark Matter Cosmogony. II. Observational Tests. *Astrophys. J.*, 510:531–540, January 1999.
- [35] L. Moscardini, S. Matarrese, F. Lucchin, and A. Messina. Non-Gaussian initial conditions in cosmological N-body simulations. II - Cold Dark Matter models. *Mon. Not. R. Astron. Soc.*, 248:424–438, February 1991.
- [36] D. H. Weinberg and S. Cole. Non-Gaussian fluctuations and the statistics of galaxy clustering. *Mon. Not. R. Astron. Soc.*, 259:652–694, December 1992.
- [37] P. Coles, L. Moscardini, F. Lucchin, S. Matarrese, and A. Messina. Skewness as a Test of Non-Gaussian Primordial Density Fluctuations. *Mon. Not. R. Astron. Soc.*, 264:749–+, October 1993.
- [38] E. Gaztanaga and P. Maehoenen. Large-Scale Clustering from Non-Gaussian Texture Models. *Astrophys. J. Lett.*, 462:L1+, May 1996.
- [39] M. White. Higher order moments of the density field in a parametrized sequence of non-Gaussian theories. *Mon. Not. R. Astron. Soc.*, 310:511–516, December 1999.
- [40] H. Mathis, J. Silk, L. M. Griffiths, and M. Kunz. Constraining cosmic microwave background consistent primordial voids with cluster evolution. *Mon. Not. R. Astron. Soc.*, 350:287–297, May 2004.
- [41] M. Grossi, E. Branchini, K. Dolag, S. Matarrese, and L. Moscardini. The mass density field in simulated non-Gaussian scenarios. *Mon. Not. R. Astron. Soc.*, 390:438–446, October 2008.
- [42] V. Desjacques, U. Seljak, and I. T. Iliev. Scale-dependent bias induced by local non-Gaussianity: a comparison to N-body simulations. *Mon. Not. R. Astron. Soc.*, 396:85–96, June 2009.
- [43] A. Pillepich, C. Porciani, and O. Hahn. Halo mass function and scale-dependent bias from N-body simulations with non-Gaussian initial conditions. *Mon. Not. R. Astron. Soc.*, 402:191–206, February 2010.
- [44] T. Nishimichi, A. Taruya, K. Koyama, and C. Sabiu. Scale Dependence of Halo Bispectrum from Non-Gaussian Initial Conditions in Cosmological N-body Simulations. *ArXiv e-prints*, November 2009.
- [45] R. Vio, P. Andreani, and W. Wamsteker. Numerical Simulation of Non-Gaussian Random Fields with Prescribed Correlation Structure. *Pub. Astron. Soc. Pac.*, 113:1009–1020, August 2001.
- [46] U. Seljak and M. Zaldarriaga. A Line-of-Sight Integration Approach to Cosmic Microwave Background Anisotropies. *Astrophys. J.*, 469:437–+, October 1996.
- [47] A. Lewis, A. Challinor, and A. Lasenby. Efficient Computation of Cosmic Microwave Background Anisotropies in Closed Friedmann-Robertson-Walker Models. *Astrophys. J.*, 538:473–476, August 2000.
- [48] P. McDonald. Primordial non-Gaussianity: Large-scale structure signature in the perturbative bias model. *Phys. Rev. D.*, 78(12):123519–+, December 2008.
- [49] V. Desjacques and U. Seljak. Signature of primordial non-Gaussianity of ϕ^3 type in the mass function and bias of dark matter haloes. *Phys. Rev. D.*, 81(2):023006–+, January 2010.
- [50] R. Juszkiewicz, F. R. Bouchet, and S. Colombi. Skew-

- ness induced by gravity. *Astrophys. J. Lett.*, 412:L9–L12, July 1993.
- [51] C. M. Baugh, E. Gaztanaga, and G. Efstathiou. A comparison of the evolution of density fields in perturbation theory and numerical simulations - II. Counts-in-cells analysis. *Mon. Not. R. Astron. Soc.*, 274:1049–1070, June 1995.
- [52] R. Scoccimarro. Transients from initial conditions: a perturbative analysis. *Mon. Not. R. Astron. Soc.*, 299:1097–1118, October 1998.
- [53] M. Crocce, S. Pueblas, and R. Scoccimarro. Transients from initial conditions in cosmological simulations. *Mon. Not. R. Astron. Soc.*, 373:369–381, November 2006.
- [54] X. Luo and D. N. Schramm. Kurtosis, skewness, and non-Gaussian cosmological density perturbations. *Astrophys. J.*, 408:33–42, May 1993.
- [55] E. L. Lokas, R. Juszkiewicz, D. H. Weinberg, and F. R. Bouchet. Kurtosis of large-scale cosmic fields. *Mon. Not. R. Astron. Soc.*, 274:730–744, June 1995.
- [56] P. J. E. Peebles. *The large-scale structure of the universe*. 1980.
- [57] J. N. Fry. The Galaxy correlation hierarchy in perturbation theory. *Astrophys. J.*, 279:499–510, April 1984.
- [58] P. Coles and C. S. Frenk. Skewness and large-scale structure. *Mon. Not. R. Astron. Soc.*, 253:727–737, December 1991.
- [59] F. R. Bouchet, R. Juszkiewicz, S. Colombi, and R. Pelat. Weakly nonlinear gravitational instability for arbitrary Omega. *Astrophys. J. Lett.*, 394:L5–L8, July 1992.
- [60] O. Lahav, M. Itoh, S. Inagaki, and Y. Suto. Non-Gaussian signatures from Gaussian initial fluctuations - Evolution of skewness and kurtosis from cosmological simulations in the highly nonlinear regime. *Astrophys. J.*, 402:387–397, January 1993.
- [61] J. N. Fry and R. J. Scherrer. Skewness in large-scale structure and non-Gaussian initial conditions. *Astrophys. J.*, 429:36–42, July 1994.
- [62] E. Gaztanaga and P. Fosalba. Cosmological perturbation theory and the spherical collapse model - II. Non-Gaussian initial conditions. *Mon. Not. R. Astron. Soc.*, 301:524–534, December 1998.
- [63] R. Scoccimarro. Gravitational Clustering from χ^2 Initial Conditions. *Astrophys. J.*, 542:1–8, October 2000.
- [64] N. Turok and D. N. Spergel. Scaling solution for cosmological sigma models at large N. *Physical Review Letters*, 66:3093–3096, June 1991.
- [65] R. Durrer, R. Juszkiewicz, M. Kunz, and J.-P. Uzan. Skewness as a probe of non-Gaussian initial conditions. *Phys. Rev. D.*, 62(2):021301–+, July 2000.
- [66] M. J. Chodorowski and F. R. Bouchet. Kurtosis in large-scale structure as a constraint on non-Gaussian initial conditions. *Mon. Not. R. Astron. Soc.*, 279:557–563, March 1996.
- [67] T. Y. Lam and R. K. Sheth. The non-linear probability distribution function in models with local primordial non-Gaussianity. *Mon. Not. R. Astron. Soc.*, 395:1743–1748, May 2009.
- [68] A. Taruya, K. Koyama, and T. Matsubara. Signature of primordial non-Gaussianity on the matter power spectrum. *Phys. Rev. D.*, 78(12):123534–+, December 2008.
- [69] E. Sefusatti. One-loop perturbative corrections to the matter and galaxy bispectrum with non-Gaussian initial conditions. *Phys. Rev. D.*, 80(12):123002–+, December 2009.
- [70] M. H. Goroff, B. Grinstein, S.-J. Rey, and M. B. Wise. Coupling of modes of cosmological mass density fluctuations. *Astrophys. J.*, 311:6–14, December 1986.
- [71] N. Makino, M. Sasaki, and Y. Suto. Analytic approach to the perturbative expansion of nonlinear gravitational fluctuations in cosmological density and velocity fields. *Phys. Rev. D.*, 46:585–602, July 1992.
- [72] T. Giannantonio and C. Porciani. Structure formation from non-Gaussian initial conditions: Multivariate biasing, statistics, and comparison with N-body simulations. *Phys. Rev. D.*, 81(6):063530–+, March 2010.
- [73] S. Matarrese and M. Pietroni. Resumming cosmic perturbations. *Journal of Cosmology and Astro-Particle Physics*, 6:26–+, June 2007.
- [74] K. Izumi and J. Soda. Renormalized Newtonian cosmic evolution with primordial non-Gaussianity. *Phys. Rev. D.*, 76(8):083517–+, October 2007.
- [75] N. Bartolo, J. P. Beltran Almeida, S. Matarrese, M. Pietroni, and A. Riotto. Signatures of Primordial non-Gaussianities in the Matter Power-Spectrum and Bispectrum: the Time-RG Approach. *ArXiv e-prints*, December 2009.
- [76] P. Catelan and L. Moscardini. Kurtosis and large-scale structure. *Astrophys. J.*, 426:14–18, May 1994.
- [77] L. Verde and A. F. Heavens. On the Trispectrum as a Gaussian Test for Cosmology. *Astrophys. J.*, 553:14–24, May 2001.
- [78] E. Sefusatti, M. Crocce, and V. Desjacques. The Matter Bispectrum in N-body Simulations with non-Gaussian Initial Conditions. *ArXiv e-prints*, February 2010.
- [79] A. Loeb and M. Zaldarriaga. Measuring the Small-Scale Power Spectrum of Cosmic Density Fluctuations through 21cm Tomography Prior to the Epoch of Structure Formation. *Physical Review Letters*, 92(21):211301–+, May 2004.
- [80] A. Cooray. Large-scale non-Gaussianities in the 21-cm background anisotropies from the era of reionization. *Mon. Not. R. Astron. Soc.*, 363:1049–1056, November 2005.
- [81] A. Pillepich, C. Porciani, and S. Matarrese. The Bispectrum of Redshifted 21 Centimeter Fluctuations from the Dark Ages. *Astrophys. J.*, 662:1–14, June 2007.
- [82] M. Bartelmann and P. Schneider. Weak gravitational lensing. *Phys. Rep.*, 340:291–472, January 2001.
- [83] F. Lucchin, S. Matarrese, A. Messina, L. Moscardini, and G. Tormen. Velocity fields in non-Gaussian cold dark matter models. *Mon. Not. R. Astron. Soc.*, 272:859–868, February 1995.
- [84] R. J. Scherrer. Linear velocity fields in non-Gaussian models for large-scale structure. *Astrophys. J.*, 390:330–337, May 1992.
- [85] R. Moessner. Statistics of peculiar velocities from cosmic strings. *Mon. Not. R. Astron. Soc.*, 277:927–932, December 1995.
- [86] P. Catelan and R. J. Scherrer. Velocity differences as a probe of non-Gaussian density fields. *Astrophys. J.*, 445:1–6, May 1995.
- [87] G. P. Holder. Measuring Cluster Peculiar Velocities and Temperatures at Centimeter and Millimeter Wavelengths. *Astrophys. J.*, 602:18–25, February 2004.
- [88] L. Kofman, E. Bertschinger, J. M. Gelb, A. Nusser,

- and A. Dekel. Evolution of one-point distributions from Gaussian initial fluctuations. *Astrophys. J.*, 420:44–57, January 1994.
- [89] A. Nusser, A. Dekel, and A. Yahil. Evidence for Gaussian Initial Fluctuations from the 1.2 Jansky IRAS Survey. *Astrophys. J.*, 449:439–, August 1995.
- [90] S. D. M. White and M. J. Rees. Core condensation in heavy halos - A two-stage theory for galaxy formation and clustering. *Mon. Not. R. Astron. Soc.*, 183:341–358, May 1978.
- [91] N. Kaiser. On the spatial correlations of Abell clusters. *Astrophys. J. Lett.*, 284:L9–L12, September 1984.
- [92] V. Desjacques. Baryon acoustic signature in the clustering of density maxima. *Phys. Rev. D.*, 78(10):103503–+, November 2008.
- [93] P. McDonald and A. Roy. Clustering of dark matter tracers: generalizing bias for the coming era of precision LSS. *Journal of Cosmology and Astro-Particle Physics*, 8:20–+, August 2009.
- [94] M. Davis, G. Efstathiou, C. S. Frenk, and S. D. M. White. The evolution of large-scale structure in a universe dominated by cold dark matter. *Astrophys. J.*, 292:371–394, May 1985.
- [95] C. Lacey and S. Cole. Merger Rates in Hierarchical Models of Galaxy Formation - Part Two - Comparison with N-Body Simulations. *Mon. Not. R. Astron. Soc.*, 271:676–+, December 1994.
- [96] Z. Lukić, D. Reed, S. Habib, and K. Heitmann. The Structure of Halos: Implications for Group and Cluster Cosmology. *Astrophys. J.*, 692:217–228, February 2009.
- [97] F. Lucchin and S. Matarrese. The effect of non-Gaussian statistics on the mass multiplicity of cosmic structures. *Astrophys. J.*, 330:535–544, July 1988.
- [98] S. Colafrancesco, F. Lucchin, and S. Matarrese. The mass function from local density maxima - Groups and clusters of galaxies. *Astrophys. J.*, 345:3–11, October 1989.
- [99] P. Coles and J. D. Barrow. Non-Gaussian statistics and the microwave background radiation. *Mon. Not. R. Astron. Soc.*, 228:407–426, September 1987.
- [100] W. H. Press and P. Schechter. Formation of Galaxies and Clusters of Galaxies by Self-Similar Gravitational Condensation. *Astrophys. J.*, 187:425–438, February 1974.
- [101] J. A. Peacock and A. F. Heavens. Alternatives to the Press-Schechter cosmological mass function. *Mon. Not. R. Astron. Soc.*, 243:133–143, March 1990.
- [102] S. Cole. Modeling galaxy formation in evolving dark matter halos. *Astrophys. J.*, 367:45–53, January 1991.
- [103] J. R. Bond, S. Cole, G. Efstathiou, and N. Kaiser. Excursion set mass functions for hierarchical Gaussian fluctuations. *Astrophys. J.*, 379:440–460, October 1991.
- [104] R. K. Sheth and G. Tormen. Large-scale bias and the peak background split. *Mon. Not. R. Astron. Soc.*, 308:119–126, September 1999.
- [105] M. Maggiore and A. Riotto. The Halo Mass Function from Excursion Set Theory. I. Gaussian fluctuations with non-markovian dependence on the smoothing scale. *ArXiv e-prints*, March 2009.
- [106] S. Matarrese, L. Verde, and R. Jimenez. The Abundance of High-Redshift Objects as a Probe of Non-Gaussian Initial Conditions. *Astrophys. J.*, 541:10–24, September 2000.
- [107] M. Lo Verde, A. Miller, S. Shandera, and L. Verde. Effects of scale-dependent non-Gaussianity on cosmological structures. *Journal of Cosmology and Astro-Particle Physics*, 4:14–+, April 2008.
- [108] P. Valageas. Mass function and bias of dark matter halos for non-Gaussian initial conditions. *ArXiv e-prints*, June 2009.
- [109] M. Grossi, K. Dolag, E. Branchini, S. Matarrese, and L. Moscardini. Evolution of massive haloes in non-Gaussian scenarios. *Mon. Not. R. Astron. Soc.*, 382:1261–1267, December 2007.
- [110] M. Grossi, L. Verde, C. Carbone, K. Dolag, E. Branchini, F. Iannuzzi, S. Matarrese, and L. Moscardini. Large-scale non-Gaussian mass function and halo bias: tests on N-body simulations. *Mon. Not. R. Astron. Soc.*, 398:321–332, September 2009.
- [111] X. Kang, P. Norberg, and J. Silk. Can a large-scale structure probe cosmic microwave background-constrained non-Gaussianity? *Mon. Not. R. Astron. Soc.*, 376:343–347, March 2007.
- [112] M. Maggiore and A. Riotto. The Halo Mass Function from Excursion Set Theory with a Non-Gaussian Trispectrum. *ArXiv e-prints*, October 2009.
- [113] V. R. Eke, S. Cole, and C. S. Frenk. Cluster evolution as a diagnostic for Omega. *Mon. Not. R. Astron. Soc.*, 282:263–280, September 1996.
- [114] M. Maggiore and A. Riotto. The Halo Mass Function from Excursion Set Theory. III. Non-Gaussian Fluctuations. *ArXiv e-prints*, March 2009.
- [115] M. Maggiore and A. Riotto. The Halo Mass Function from Excursion Set Theory. II. The Diffusing Barrier. *ArXiv e-prints*, March 2009.
- [116] B. E. Robertson, A. V. Kravtsov, J. Tinker, and A. R. Zentner. Collapse Barriers and Halo Abundance: Testing the Excursion Set Ansatz. *Astrophys. J.*, 696:636–652, May 2009.
- [117] R. K. Sheth and G. Tormen. An excursion set model of hierarchical clustering: ellipsoidal collapse and the moving barrier. *Mon. Not. R. Astron. Soc.*, 329:61–75, January 2002.
- [118] T. Y. Lam and R. K. Sheth. Halo abundances in the f_{nl} model. *Mon. Not. R. Astron. Soc.*, 398:2143–2151, October 2009.
- [119] T. Y. Lam, R. K. Sheth, and V. Desjacques. The initial shear field in models with primordial local non-Gaussianity and implications for halo and void abundances. *Mon. Not. R. Astron. Soc.*, 399:1482–1494, November 2009.
- [120] P. P. Avelino and P. T. P. Viana. The cloud-in-cloud problem for non-Gaussian density fields. *Mon. Not. R. Astron. Soc.*, 314:354–358, May 2000.
- [121] K. T. Inoue and M. Nagashima. Analytic Approach to the Cloud-in-Cloud Problem for Non-Gaussian Density Fluctuations. *Astrophys. J.*, 574:9–18, July 2002.
- [122] R. K. Sheth, H. J. Mo, and G. Tormen. Ellipsoidal collapse and an improved model for the number and spatial distribution of dark matter haloes. *Mon. Not. R. Astron. Soc.*, 323:1–12, May 2001.
- [123] V. Desjacques. Environmental dependence in the ellipsoidal collapse model. *Mon. Not. R. Astron. Soc.*, 388:638–658, August 2008.
- [124] E. Rozo, R. H. Wechsler, B. P. Koester, A. E. Evrard,

- and T. A. McKay. Optically-Selected Cluster Catalogs as a Precision Cosmology Tool. *ArXiv Astrophysics e-prints*, March 2007.
- [125] S. Matarrese, F. Lucchin, and S. A. Bonometto. A path-integral approach to large-scale matter distribution originated by non-Gaussian fluctuations. *Astrophys. J. Lett.*, 310:L21–L26, November 1986.
- [126] P. Catelan, F. Lucchin, and S. Matarrese. Peak number density of non-Gaussian random fields. *Physical Review Letters*, 61:267–270, July 1988.
- [127] S. Borgani and S. A. Bonometto. Galaxy density in biased theories of galaxy origin. *Astron. Astrophys.*, 215:17–20, May 1989.
- [128] S. Matarrese, F. Lucchin, A. Messina, and L. Moscardini. Non-Gaussian initial conditions in cosmological N-body simulations. III - Groups in Cold Dark Matter models. *Mon. Not. R. Astron. Soc.*, 253:35–46, November 1991.
- [129] C. Park, D. N. Spergel, and N. Turok. Large-scale structure in a texture-seeded cold dark matter cosmogony. *Astrophys. J. Lett.*, 372:L53–L57, May 1991.
- [130] S. Borgani, P. Coles, L. Moscardini, and M. Plionis. The Angular Distribution of Clusters in Skewed CDM Models / Cold Dark Matter. *Mon. Not. R. Astron. Soc.*, 266:524–+, January 1994.
- [131] H. Mathis, J. M. Diego, and J. Silk. The case for non-Gaussianity on cluster scales. *Mon. Not. R. Astron. Soc.*, 353:681–688, September 2004.
- [132] J. Robinson and J. E. Baker. Evolution of the cluster abundance in non-Gaussian models. *Mon. Not. R. Astron. Soc.*, 311:781–792, February 2000.
- [133] R. Stanek, A. E. Evrard, H. Böhringer, P. Schuecker, and B. Nord. The X-Ray Luminosity-Mass Relation for Local Clusters of Galaxies. *Astrophys. J.*, 648:956–968, September 2006.
- [134] D. Nagai. The Impact of Galaxy Formation on the Sunyaev-Zel’dovich Effect of Galaxy Clusters. *Astrophys. J.*, 650:538–549, October 2006.
- [135] W. A. Chiu, J. P. Ostriker, and M. A. Strauss. Using Cluster Abundances and Peculiar Velocities to Test the Gaussianity of the Cosmological Density Field. *Astrophys. J.*, 494:479–+, February 1998.
- [136] A. J. Benson, C. Reichardt, and M. Kamionkowski. Statistics of Sunyaev-Zel’dovich cluster surveys. *Mon. Not. R. Astron. Soc.*, 331:71–84, March 2002.
- [137] S. Sadeh, Y. Rephaeli, and J. Silk. Impact of a non-Gaussian density field on Sunyaev-Zeldovich observables. *Mon. Not. R. Astron. Soc.*, 368:1583–1598, June 2006.
- [138] S. Sadeh, Y. Rephaeli, and J. Silk. Cluster abundances and Sunyaev-Zel’dovich power spectra: effects of non-Gaussianity and early dark energy. *Mon. Not. R. Astron. Soc.*, 380:637–645, September 2007.
- [139] E. Sefusatti, C. Vale, K. Kadota, and J. Frieman. Primordial Non-Gaussianity and Dark Energy Constraints from Cluster Surveys. *Astrophys. J.*, 658:669–679, April 2007.
- [140] C. Fedeli, L. Moscardini, and S. Matarrese. The clustering of galaxy clusters in cosmological models with non-Gaussian initial conditions: predictions for future surveys. *Mon. Not. R. Astron. Soc.*, 397:1125–1137, August 2009.
- [141] M. Roncarelli, L. Moscardini, E. Branchini, K. Dolag, M. Grossi, F. Iannuzzi, and S. Matarrese. Imprints of primordial non-Gaussianities in X-ray and SZ signals from galaxy clusters. *ArXiv e-prints*, September 2009.
- [142] J. Oukbir, J. G. Bartlett, and A. Blanchard. X-ray galaxy clusters: constraints on models of galaxy formation. *Astron. Astrophys.*, 320:365–377, April 1997.
- [143] J. P. Henry. Measuring Cosmological Parameters from the Evolution of Cluster X-Ray Temperatures. *Astrophys. J.*, 534:565–580, May 2000.
- [144] A. Amara and A. Refregier. Power spectrum normalization and the non-Gaussian halo model. *Mon. Not. R. Astron. Soc.*, 351:375–383, June 2004.
- [145] R. Mandelbaum and U. Seljak. A robust lower limit on the amplitude of matter fluctuations in the universe from cluster abundance and weak lensing. *Journal of Cosmology and Astro-Particle Physics*, 6:24–+, June 2007.
- [146] M. Kamionkowski, L. Verde, and R. Jimenez. The void abundance with non-gaussian primordial perturbations. *Journal of Cosmology and Astro-Particle Physics*, 1:10–+, January 2009.
- [147] A. G. Doroshkevich. The space structure of perturbations and the origin of rotation of galaxies in the theory of fluctuation. *Astrofizika*, 6:581–600, 1970.
- [148] H. Song and J. Lee. The Mass Function of Void Groups as a Probe of Primordial Non-Gaussianity. *Astrophys. J. Lett.*, 701:L25–L28, August 2009.
- [149] R. K. Sheth and R. van de Weygaert. A hierarchy of voids: much ado about nothing. *Mon. Not. R. Astron. Soc.*, 350:517–538, May 2004.
- [150] J. M. Colberg, F. Pearce, C. Foster, E. Platen, R. Brunino, M. Neyrinck, S. Basilakos, A. Fairall, H. Feldman, S. Gottlöber, O. Hahn, F. Hoyle, V. Müller, L. Nelson, M. Plionis, C. Porciani, S. Shandarin, M. S. Vogeley, and R. van de Weygaert. The Aspen-Amsterdam void finder comparison project. *Mon. Not. R. Astron. Soc.*, 387:933–944, June 2008.
- [151] A. Dressler. Galaxy morphology in rich clusters - Implications for the formation and evolution of galaxies. *Astrophys. J.*, 236:351–365, March 1980.
- [152] P. J. E. Peebles. The sequence of cosmogony and the nature of primeval departures from homogeneity. *Astrophys. J.*, 274:1–6, November 1983.
- [153] N. A. Bahcall and R. M. Soneira. The spatial correlation function of rich clusters of galaxies. *Astrophys. J.*, 270:20–38, July 1983.
- [154] A. A. Klypin and A. I. Kopylov. The Spatial Covariance Function for Rich Clusters of Galaxies. *Soviet Astronomy Letters*, 9:41–+, February 1983.
- [155] B. Grinstein and M. B. Wise. Non-Gaussian fluctuations and the correlations of galaxies or rich clusters of galaxies. *Astrophys. J.*, 310:19–22, November 1986.
- [156] A. P. A. Andrade, A. L. B. Ribeiro, and C. A. Wuensche. High order correction terms for the peak-peak correlation function in nearly-Gaussian models. *Astron. Astrophys.*, 457:385–391, October 2006.
- [157] A. Slosar, C. Hirata, U. Seljak, S. Ho, and N. Padmanabhan. Constraints on local primordial non-Gaussianity from large scale structure. *Journal of Cosmology and Astro-Particle Physics*, 8:31–+, August 2008.
- [158] S. Matarrese and L. Verde. The Effect of Primordial Non-Gaussianity on Halo Bias. *Astrophys. J. Lett.*, 677:L77–L80, April 2008.
- [159] J. M. Bardeen, J. R. Bond, N. Kaiser, and A. S. Szalay. The statistics of peaks of Gaussian random fields.

- Astrophys. J.* , 304:15–61, May 1986.
- [160] S. Cole and N. Kaiser. Biased clustering in the cold dark matter cosmogony. *Mon. Not. R. Astron. Soc.* , 237:1127–1146, April 1989.
- [161] N. Afshordi and A. J. Tolley. Primordial non-Gaussianity, statistics of collapsed objects, and the integrated Sachs-Wolfe effect. *Phys. Rev. D.* , 78(12):123507–+, December 2008.
- [162] H. J. Mo and S. D. M. White. An analytic model for the spatial clustering of dark matter haloes. *Mon. Not. R. Astron. Soc.* , 282:347–361, September 1996.
- [163] R. Y. Cen, J. P. Ostriker, D. N. Spergel, and N. Turok. A hydrodynamic approach to cosmology - Texture-seeded cold dark matter and hot dark matter cosmogonies. *Astrophys. J.* , 383:1–18, December 1991.
- [164] L. Verde and S. Matarrese. Detectability of the Effect of Inflationary Non-Gaussianity on Halo Bias. *Astrophys. J. Lett.* , 706:L91–L95, November 2009.
- [165] E. Hatziminaoglou, G. Mathez, J.-M. Solanes, A. Manrique, and E. Salvador-Solé. Major mergers of haloes, the growth of massive black holes and the evolving luminosity function of quasars. *Mon. Not. R. Astron. Soc.* , 343:692–704, August 2003.
- [166] P. F. Hopkins, L. Hernquist, T. J. Cox, T. Di Matteo, P. Martini, B. Robertson, and V. Springel. Black Holes in Galaxy Mergers: Evolution of Quasars. *Astrophys. J.* , 630:705–715, September 2005.
- [167] S. Bonoli, F. Shankar, S. White, V. Springel, and S. Wyithe. On merger bias and the clustering of quasars. *ArXiv e-prints*, August 2009.
- [168] N. Bartolo, S. Matarrese, and A. Riotto. Signatures of primordial non-Gaussianity in the large-scale structure of the universe. *Journal of Cosmology and Astro-Particle Physics*, 10:10–+, October 2005.
- [169] D. Wands and A. Slosar. Scale-dependent bias from primordial non-Gaussianity in general relativity. *Phys. Rev. D.* , 79(12):123507–+, June 2009.
- [170] J. N. Fry and E. Gaztanaga. Biasing and hierarchical statistics in large-scale structure. *Astrophys. J.* , 413:447–452, August 1993.
- [171] N. Kaiser. Clustering in real space and in redshift space. *Mon. Not. R. Astron. Soc.* , 227:1–21, July 1987.
- [172] A. J. S. Hamilton. Linear Redshift Distortions: a Review. In D. Hamilton, editor, *The Evolving Universe*, volume 231 of *Astrophysics and Space Science Library*, pages 185–+, 1998.
- [173] T. Y. Lam, V. Desjacques, and R. K. Sheth. The non-linear redshift space probability distribution function in models with local primordial non-Gaussianity. *Mon. Not. R. Astron. Soc.* , 402:2397–2402, March 2010.
- [174] H. A. Feldman, N. Kaiser, and J. A. Peacock. Power-spectrum analysis of three-dimensional redshift surveys. *Astrophys. J.* , 426:23–37, May 1994.
- [175] U. Seljak. Extracting Primordial Non-Gaussianity without Cosmic Variance. *Physical Review Letters*, 102(2):021302–+, January 2009.
- [176] P. McDonald and U. Seljak. How to evade the sample variance limit on measurements of redshift-space distortions. *Journal of Cosmology and Astro-Particle Physics*, 10:7–+, October 2009.
- [177] A. Slosar. Optimal weighting in f_{NL} constraints from large scale structure in an idealised case. *Journal of Cosmology and Astro-Particle Physics*, 3:4–+, March 2009.
- [178] U. Seljak, N. Hamaus, and V. Desjacques. How to Suppress the Shot Noise in Galaxy Surveys. *Physical Review Letters*, 103(9):091303–+, August 2009.
- [179] N. Hamaus, et al. in preparation. 2010.
- [180] Z. Fan and J. M. Bardeen. Distributions of Fourier modes of cosmological density fields. *Phys. Rev. D.* , 51:6714–6721, June 1995.
- [181] A. J. Stirling and J. A. Peacock. Power correlations in cosmology: limits on primordial non-Gaussian density fields. *Mon. Not. R. Astron. Soc.* , 283:L99+, December 1996.
- [182] E. Sefusatti and E. Komatsu. Bispectrum of galaxies from high-redshift galaxy surveys: Primordial non-Gaussianity and nonlinear galaxy bias. *Phys. Rev. D.* , 76(8):083004–+, October 2007.
- [183] D. Jeong and E. Komatsu. Primordial Non-Gaussianity, Scale-dependent Bias, and the Bispectrum of Galaxies. *Astrophys. J.* , 703:1230–1248, October 2009.
- [184] E. Gaztanaga. N-point correlation functions in the CfA and SSRS redshift distribution of galaxies. *Astrophys. J. Lett.* , 398:L17–L20, October 1992.
- [185] E. Gaztanaga and J. Yokoyama. Probing the statistics of primordial fluctuations and their evolution. *Astrophys. J.* , 403:450–465, February 1993.
- [186] F. R. Bouchet, M. A. Strauss, M. Davis, K. B. Fisher, A. Yahil, and J. P. Huchra. Moments of the Counts Distribution in the 1.2 Jansky IRAS Galaxy Redshift Survey. *Astrophys. J.* , 417:36–+, November 1993.
- [187] S. Luo and E. Vishniac. Bayesian approaches to testing the nature of primordial density fluctuation. *Astrophys. J.* , 443:469–478, April 1995.
- [188] D. J. Croton, E. Gaztañaga, C. M. Baugh, P. Norberg, M. Colless, I. K. Baldry, J. Bland-Hawthorn, T. Bridges, R. Cannon, S. Cole, C. Collins, W. Couch, G. Dalton, R. De Propris, S. P. Driver, G. Efstathiou, R. S. Ellis, C. S. Frenk, K. Glazebrook, C. Jackson, O. Lahav, I. Lewis, S. Lumsden, S. Maddox, D. Madgwick, J. A. Peacock, B. A. Peterson, W. Sutherland, and K. Taylor. The 2dF Galaxy Redshift Survey: higher-order galaxy correlation functions. *Mon. Not. R. Astron. Soc.* , 352:1232–1244, August 2004.
- [189] W. J. Frith, P. J. Outram, and T. Shanks. High-order 2MASS galaxy correlation functions: probing the Gaussianity of the primordial density field. *Mon. Not. R. Astron. Soc.* , 373:759–768, December 2006.
- [190] T. Matsubara and Y. Suto. Nonlinear Evolution of Genus in a Primordial Random Gaussian Density Field. *Astrophys. J.* , 460:51–+, March 1996.
- [191] P. Coles, L. Moscardini, M. Plionis, F. Lucchin, S. Matarrese, and A. Messina. Topology in two dimensions. IV - CDM models with non-Gaussian initial conditions. *Mon. Not. R. Astron. Soc.* , 260:572–588, February 1993.
- [192] T. Matsubara and J. Yokoyama. Genus Statistics of the Large-Scale Structure with Non-Gaussian Density Fields. *Astrophys. J.* , 463:409–+, June 1996.
- [193] C. Hikage, A. Taruya, and Y. Suto. Genus Statistics for Galaxy Clusters and Nonlinear Biasing of Dark Matter Halos. *Astrophys. J.* , 556:641–652, August 2001.
- [194] C. Hikage, P. Coles, M. Grossi, L. Moscardini, K. Dolag, E. Branchini, and S. Matarrese. The effect of primordial

- non-Gaussianity on the topology of large-scale structure. *Mon. Not. R. Astron. Soc.*, 385:1613–1620, April 2008.
- [195] J. R. Gott, III, D. C. Hambrick, M. S. Vogeley, J. Kim, C. Park, Y.-Y. Choi, R. Cen, J. P. Ostriker, and K. Nagamine. Genus Topology of Structure in the Sloan Digital Sky Survey: Model Testing. *Astrophys. J.*, 675:16–28, March 2008.
- [196] J. B. James, M. Colless, G. F. Lewis, and J. A. Peacock. Topology of non-linear structure in the 2dF Galaxy Redshift Survey. *Mon. Not. R. Astron. Soc.*, 394:454–466, March 2009.
- [197] X. Chen, A. Cooray, N. Yoshida, and N. Sugiyama. Can non-Gaussian cosmological models explain the WMAP high optical depth for reionization? *Mon. Not. R. Astron. Soc.*, 346:L31–L35, December 2003.
- [198] P. P. Avelino and A. R. Liddle. Cosmic reionization constraints on the nature of cosmological perturbations. *Mon. Not. R. Astron. Soc.*, 371:1755–1759, October 2006.
- [199] D. Crociani, L. Moscardini, M. Viel, and S. Matarrese. The effects of primordial non-Gaussianity on the cosmological reionization. *Mon. Not. R. Astron. Soc.*, 394:133–141, March 2009.
- [200] M. Viel, E. Branchini, K. Dolag, M. Grossi, S. Matarrese, and L. Moscardini. Primordial non-Gaussianities in the intergalactic medium. *Mon. Not. R. Astron. Soc.*, 393:774–782, March 2009.
- [201] S. Ho, et al. in preparation. 2010.
- [202] J. E. Gunn and B. A. Peterson. On the Density of Neutral Hydrogen in Intergalactic Space. *Astrophys. J.*, 142:1633–1641, November 1965.
- [203] R. A. C. Croft, D. H. Weinberg, N. Katz, and L. Hernquist. Recovery of the Power Spectrum of Mass Fluctuations from Observations of the Ly alpha Forest. *Astrophys. J.*, 495:44–+, March 1998.
- [204] M. Zaldarriaga, R. Scoccimarro, and L. Hui. Inferring the Linear Power Spectrum from the Ly α Forest. *Astrophys. J.*, 590:1–7, June 2003.
- [205] P. McDonald. Toward a Measurement of the Cosmological Geometry at $z \sim 2$: Predicting Ly α Forest Correlation in Three Dimensions and the Potential of Future Data Sets. *Astrophys. J.*, 585:34–51, March 2003.
- [206] P. Coles and B. Jones. A lognormal model for the cosmological mass distribution. *Mon. Not. R. Astron. Soc.*, 248:1–13, January 1991.
- [207] H. Bi and A. F. Davidsen. Evolution of Structure in the Intergalactic Medium and the Nature of the Ly alpha Forest. *Astrophys. J.*, 479:523–+, April 1997.
- [208] E. Komatsu, K. M. Smith, J. Dunkley, C. L. Bennett, B. Gold, G. Hinshaw, N. Jarosik, D. Larson, M. R.olta, L. Page, D. N. Spergel, M. Halpern, R. S. Hill, A. Kogut, M. Limon, S. S. Meyer, N. Odegard, G. S. Tucker, J. L. Weiland, E. Wollack, and E. L. Wright. Seven-Year Wilkinson Microwave Anisotropy Probe (WMAP) Observations: Cosmological Interpretation. *ArXiv e-prints*, January 2010.
- [209] J. A. Frieman and E. Gaztañaga. The Projected Three-Point Correlation Function: Theory and Observations. *Astrophys. J. Lett.*, 521:L83–L86, August 1999.
- [210] R. Scoccimarro, H. A. Feldman, J. N. Fry, and J. A. Frieman. The Bispectrum of IRAS Redshift Catalogs. *Astrophys. J.*, 546:652–664, January 2001.
- [211] G. V. Kulkarni, R. C. Nichol, R. K. Sheth, H.-J. Seo, D. J. Eisenstein, and A. Gray. The three-point correlation function of luminous red galaxies in the Sloan Digital Sky Survey. *Mon. Not. R. Astron. Soc.*, 378:1196–1206, July 2007.
- [212] E. Gaztañaga, A. Cabré, F. Castander, M. Crocce, and P. Fosalba. Clustering of luminous red galaxies - III. Baryon acoustic peak in the three-point correlation. *Mon. Not. R. Astron. Soc.*, 399:801–811, October 2009.
- [213] J. A. Willick. Constraints on Primordial Non-Gaussianity from the High-Redshift Cluster MS 1054-03. *Astrophys. J.*, 530:80–95, February 2000.
- [214] R. Jimenez and L. Verde. Implications for primordial non-Gaussianity (f_{NL}) from weak lensing masses of high- z galaxy clusters. *Phys. Rev. D.*, 80(12):127302–+, December 2009.
- [215] B. Sartoris, S. Borgani, C. Fedeli, S. Matarrese, L. Moscardini, P. Rosati, and J. Weller. The potential of X-ray cluster surveys to constrain primordial non-Gaussianity. *ArXiv e-prints*, March 2010.
- [216] D. Jeong, E. Komatsu, and B. Jain. Galaxy-CMB and galaxy-galaxy lensing on large scales: Sensitivity to primordial non-Gaussianity. *Phys. Rev. D.*, 80(12):123527–+, December 2009.
- [217] C. Fedeli and L. Moscardini. Cosmic shear statistics in cosmologies with non-Gaussian initial conditions. *ArXiv e-prints*, December 2009.
- [218] C. Carbone, L. Verde, and S. Matarrese. Non-Gaussian Halo Bias and Future Galaxy Surveys. *Astrophys. J. Lett.*, 684:L1–L4, September 2008.
- [219] M. Takada and B. Jain. Cosmological parameters from lensing power spectrum and bispectrum tomography. *Mon. Not. R. Astron. Soc.*, 348:897–915, March 2004.
- [220] Y. Gong, X. Wang, Z. Zheng, and X.-L. Chen. Primordial non-Gaussianity from LAMOST surveys. *Research in Astronomy and Astrophysics*, 10:107–115, February 2010.
- [221] E. Sefusatti, M. Liguori, A. P. S. Yadav, M. G. Jackson, and E. Pajer. Constraining running non-gaussianity. *Journal of Cosmology and Astro-Particle Physics*, 12:22–+, December 2009.
- [222] C. Carbone, O. Mena, and L. Verde. Cosmological Parameters Degeneracies and Non-Gaussian Halo Bias. *ArXiv e-prints*, March 2010.
- [223] M. Oguri. Self-Calibrated Cluster Counts as a Probe of Primordial Non-Gaussianity. *Physical Review Letters*, 102(21):211301–+, May 2009.
- [224] C. Cunha, D. Huterer, and O. Dore. Primordial non-Gaussianity from the covariance of galaxy cluster counts. *ArXiv e-prints*, March 2010.